

**CICLOSTRATIGRAPHY OF SEDIMENTARY RECORDS IN SOUTHERN ALBACORA
FIELD, CAMPOS BASIN, BRAZIL**

Ciro Climaco Rodrigues

Dissertation presented to the Graduate Program in Geophysics at the National Observatory, as part of the requirements for obtaining the title of Master in Geophysics.

Advised by:

Dr. Daniel Ribeiro Franco (ON/MCTI)

Co-Advisors:

Dr. Natália Braun dos Santos (ON/MCTI) and

Dr. Mingsong Li (Peking University)

RIO DE JANEIRO, RJ - BRASIL

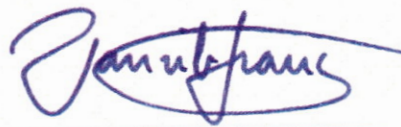
JUNHO DE 2023

“CICLOSTRATIGRAPHY OF SEDIMENTARY RECORDS IN SOUTHERN
ALBACORA FIELD, CAMPOS BASIN, BRAZIL”

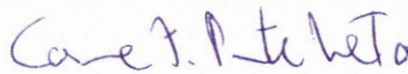
Ciro Climaco Rodrigues

DISSERTAÇÃO SUBMETIDA AO CORPO DOCENTE DO PROGRAMA DE
PÓS-GRADUAÇÃO EM GEOFÍSICA DO OBSERVATÓRIO NACIONAL COMO
PARTE DOS REQUISITOS NECESSÁRIOS PARA A OBTENÇÃO DO GRAU
DE MESTRE EM GEOFÍSICA.

Aprovada por:



Dr. Daniel Ribeiro Franco - (Orientador) - (ON)



Dr. Cosme Ferreira da Ponte Neto – (ON)



Dra. Joice Cagliari - (UNISINOS)

RIO DE JANEIRO – BRASIL

30 DE JUNHO DE 2023

Rodrigues, C i r o C l i m a c o

Ciclostratigraphy of sedimentary records in southern
Albacora field, Campos Basin, Brazil /Ciro Climaco

Rodrigues. – Rio de Janeiro: ON, 2023.

??, 87 p.: il.; 29, 7cm.

Orientador(a): Daniel Ribeiro Franco

Co-orientadores: Minsong Li

Natália Braun dos Santos

Dissertação (mestrado) – ON/Programa de Pós-
graduação em Geofísica, 2023.

Referências Bibliográficas: p. 60– 73.

1. Bacia de Campos. 2. Cicloestratigrafia.
3. Interpretação Sísmica. I. Santos, Natália Braun *et al.*
II. Observatório Nacional, Programa de Pós-graduação em
Geofísica. III. Título.

Acknowledgments

Firstly, I would like to express my gratitude to my grandmother, Manuela, who always insisted that I pursue my studies, as she believed that acquiring knowledge is the path to achieving dreams. I would like to thank my mother, Roseana, my sister, Ana Manoela, and Linda Cristina, who never let me give up on my master's degree during the first quarter of this course. I am also grateful to my father, Ênio, my Aunt Ana Rosa, and my godfather, Edson, the latter two who visited and supported me during my first attempt at a master's degree 13 years ago.

I extend my deepest gratitude to my co-advisor, Dr. Natália Braun, whose patience was crucial to this study, and without her, this moment would not have been possible. I would like to thank my advisor, Dr. Daniel Franco, for his guidance and teachings in cyclostratigraphy. Thanks to my co-advisor, Mingsong Li, for providing this opportunity and for resolving significant issues and challenges in this work.

I express my gratitude to the geologist and colleague André de Gasperi for the project, the teachings, and the confidence in executing it. I thank geologist Daniel Galvão for recommending André to me and for helping me during my master's degree. I acknowledge the geologists Ana Natália and Lucio Tukitake for their consultations on rock dating.

I am thankful to the Brazilian National Agency for Petroleum, Natural Gas and Biofuels (ANP) for providing the data. I also want to extend my gratitude to the federal government and public institutions, as without them, I would not be experiencing this moment, as I am an employee of Petrobras, which provided me with the infrastructure and the necessary leave, in addition to being a postgraduate student at Observatório Nacional-MCTI.

I would like to express my gratitude to the reservoir geophysics team at Petrobras, especially my manager, Rui, and my friends Alexandre Maul and Marcos Sebastião, who encouraged me to pursue my master's degree again. I am grateful to Mônica Muzzette for reviewing the resolution work, which is a part of this research. I extend my thanks to the geophysicists and friends Anderson Santiago, with whom things come easy, and Olavo Linhares, for assisting me with materials related to the geology of the studied area.

I express my gratitude to the cyclostratigraphy team at Observatório Nacional: Mariana Aragão, Mariane Candido, Raysa Rocha, Gabriella Fazzio, Jonatã Teixeira, and Luiz Henrique, as well as the researcher from UFF, Thiago Pereira dos Santos. I am grateful to my classmates and those from the subsequent class, as I took courses with them, especially my friend Gabriel Nogueira.

Lastly, I would like to offer my final thanks to those who supported me throughout this journey: Juliana Rodrigues, Giovana Larrat, Giulia Larrat, Kaue Paraense, Caio Peixoto, Elyston Carlos Melo Moura, Alberto Akel, André Andrade, Kivia Gomes, Larissa Beatriz, Carlos Prado, Thiago Mattos, Luciana Cavalcante, Gustavo Vasconcelos, Rodrigo Pontes, Daniel Campos, Rafael Rodrigues, João Wiessmann, Tiago Sobrinho, Dorivan Araújo, Michele Ramos, Antônio Carlos Rodrigues, Ênio Rodrigues filho, and João Rodrigues. I am grateful to the dog Farofa, who entered my car on a rainy day to take care of me during this period.

Resumo de dissertação apresentado ao Programa de Pós-Graduação em Geofísica do Observatório Nacional como parte dos requisitos necessários para a obtenção do título de Mestre em Geofísica.

CICLOSTRATIGRAPHY OF SEDIMENTARY RECORDS IN ALBACORA FIELD,
CAMPOS BASIN

Ciro Clímaco Rodrigues

Junho/2023

A presente dissertação integra interpretações sísmicas e cicloestratigráficas realizadas na região de quebra de talude da porção norte da Bacia de Campos, Brasil. Para tal, utilizou-se dados de raio gama de três poços, dispostos em um perfil *dip*, e aquisições sísmicas 3D localizados nos depósitos miocênicos da jazida de hidrocarbonetos de Albacora. Apenas o poço localizado mais proximal (1-RJS-297) possui controle cronoestratigráfico (biozonas) para a geração da escala de tempo astronômica. Os outros dois poços, não possuem registro de *tie-points* e, portanto, tinham escalas de tempo astronômica flutuantes. Esta questão foi contornada a partir da associação de idades para refletores sísmicos comum a todos os poços. A associação destas idades foi por meio da cicloestratigrafia e das biozonas presentes no poço 1-RJS-297. Os resultados das análises cicloestratigráficas demonstraram que há a influência de forçantes orbitais modulando a deposição dos sedimentos. A análise espectral em conjunto com a análise harmônica evolucionária revelou ciclos sedimentares interpretados como ciclos de excentricidade longa e curta, obliquidade e precessão. As análises de taxa de acumulação de sedimentos confirmaram a modulação por ciclos de Milankovitch e geraram valores entre 28 e 45 cm/kyr, o que corrobora com a literatura. A interpretação sísmica foi essencial para a correlação entre poços e para a amarração dos ciclos de Milancovitch no tempo geológico. A integração destes dois métodos de análise de depósitos, cicloestratigrafia e sismoestratigrafia, possibilitou a realização de uma cronoestratigrafia 2D de alta resolução para a área de estudo compreendendo um período de 3 Myr. A série de dados estudada compreende os depósitos do Mioceno médio e registra o

Ótimo Climático do Mioceno e as importantes quedas do nível do mar que o delimitam. A interpretação destes registros forneceu importantes inferências sobre a evolução sedimentar e paleoclimática da região.

Abstract of the dissertation presented to the National Observatory's Graduate Program in Geophysics as a partial fulfillment of the requirements for the degree of Master in Geophysics.

CICLOSTRATIGRAPHY OF SEDIMENTARY RECORDS IN ALBACORA FIELD,
CAMPOS BASIN

Ciro Climaco Rodrigues

In this work, we integrate seismic and cyclostratigraphic interpretations carried out in the thinning region of the northern portion of the Campos Basin, Brazil. For this purpose, gamma-ray data from three wells, arranged in a dip profile, and 3D seismic acquisitions located in the Miocene deposits of the Albacora hydrocarbon field were used. Only the most onshore well (1-RJS-297) has chronostratigraphic control through biozones that have been used as tie-points in the generation of the astronomical time scale. The other two wells did not have tie-point records and therefore had floating astronomical time scale. This issue has been addressed by associating ages with seismic reflectors common to all wells. The association between these ages was made through cyclostratigraphy and the biozones present in well 1-RJS-297. The results of cyclostratigraphic analyses have shown that orbital forces modulate the deposition of sediments. Spectral analysis, in conjunction with evolutionary harmonic analysis, revealed sedimentary cycles interpreted as cycles of long and short eccentricity, obliquity, and precession. Sediment accumulation rate analyses confirmed Milankovitch cycle modulation and generated values between 28 and 45 cm/kyr, which corroborate the literature. Thus, seismic interpretation was essential for the correlation between wells and the establishment of Milankovitch cycles in geological time. The integration of these two methods of deposit analysis, sismostratigraphic and cyclostratigraphic, made it possible to perform a high-resolution 2D chronostratigraphy for the study area, comprising a period of 3 Myr. The data series studied comprise the deposits of the middle Miocene and record the Optimal Climate of the Miocene, as well as the significant sea-level

falls that define it. The interpretation of these records provided important inferences on the sedimentary and paleoclimatic evolution of the region.

RIO DE JANEIRO, RJ - BRASIL
JUNHO DE 2023

Contents

RIO DE JANEIRO, RJ - BRASIL

JUNHO DE 2023

	ii
Acknowledgments	iv
List of Figures	xii
List of Tables	xiii
List of Abbreviations	xiv
General Outlines	1
Chapter 1	2
Introduction	2
Objectives	4
Chapter 2	5
Geological Setting	5
Chapter 3	8
Chronostratigraphy of Albacora Terrace	8
Chapter 4	11
Cyclostratigraphy: theoretical background	11
4.1 The climate spectrum	11
4.2 Milankovitch Cycles	14
4.3 The astronomical time scale: potential for basin chronostratigraphic frameworks astrochronology	19
Chapter 5	21
Data and Methods	21
5.1 Data Acquisition	21
5.2 Seismic Interpretation	22
5.3 Cyclostratigraphy Analysis	23
5.3.1 Time-series Analysis	24
5.3.2 Evolutionary Harmonic Analysis	26

5.3.2 Filters and Astronomical Tunning	26
Chapter 6	30
About the manuscript “INTEGRATION OF SEISMIC AND CYCLOSTRATIGRAPHY FOR HIGH RESOLUTION CHRONOSTRATIGRAPHIC CORRELATION: THE ALBACORA RING FENCE, CAMPOS BASIN, BRAZIL”	30
Chapter 7	31
INTEGRATION OF SEISMIC AND CYCLOSTRATIGRAPHY FOR HIGH RESOLUTION CHRONOSTRATIGRAPHIC CORRELATION: THE ALBACORA RING FENCE, CAMPOS BASIN, BRAZIL	31
Chapter 8	61
Final Considerations	61
Bibliography	62

List of Figures

Figure 1 - São Paulo Plateau and highlighted 3D seismic survey limits with sea bottom surface and wells. The studied area is represented by 2D seismic section A - A' and wells 1-RJS-297, 4-RJS-330A and 3-AB-68 (modified from Almeida and Kowsmann, 2014).....	2
Figure 2- Campos Basin stratigraphic chart. The study marked in red square (Modified from Winter et al., 2017).....	7
Figure 3 - Biozone distributions. The species with asterisks have their disappearances delimiting biozones in the Brazilian continental margin. Highlighted species (red rectangle) are the biozones that help tie cycles in time in study (modified from Batiston et al., 2016)	10
Figure 4 - Periodicities related to the climate spectrum (Fragoso et al., 2021).....	13
Figure 5 - Milankovitch Cycles quasi-periodicity a) Obliquity, b) Eccentricity, c) Precession and d) the result of then on insolation. (Fragoso et al., 2021).....	16
Figure 6 - Representation of the different obliquity configurations (Rodrigues, 2018).....	17
Figure 7 - Representation of the different configurations of the climatic precession. On the left the axial precession and on the right the apsidal precession (Rodrigues, 2018).....	18
Figure 8 - Cyclostratigraphic analysis workflow.....	24

List of Tables

Table 1 - Main frequencies and periods index over 0-4Ma (Modified Hinnov et al., 2013).....	28
---	----

List of Abbreviations

ATS: Astronomical Time Scale

ASM: Average Spectral Misfit

COCO: Correlation Coefficient

DFT: Discrete Fourier Transform

eCOCO: Evolutionary Correlation Coefficient

EHA: Evolutionary harmonic analysis

ENSO: El Niño/Southern Oscillation

FFT: Fast Fourier Transform

GR: Gamma Ray

IL: Inline

MTM: Mutiple-Taper Method

NAO: North Atlantic Oscillation

SAR: Sediment Accumulation Rate

XL: CrossLine

General Outlines

This dissertation was prepared in the form of a scientific article following the norms of the Graduate Program in Geophysics of the National Observatory. The research is presented in six chapters, where I initially addressed the generalities and theoretical concepts of the work. The initial chapters contain an introduction, objectives, the study area's geological characterization, cyclostratigraphic concepts, and details of the methods used. The last chapters of the dissertation comprise the manuscript entitled "INTEGRATION OF SEISMIC AND CYCLOSTRATIGRAPHY FOR HIGH RESOLUTION CHRONOSTRATIGRAPHIC CORRELATION: THE ABACORA RING FENCE, CAMPOS BASIN, BRAZIL," submitted to the international, peer-reviewed journal *Marine and Petroleum Geology* and the final considerations about the dissertation.

Chapter 1

Introduction

The Campos Basin is situated between the northern coast of Rio de Janeiro and the southern coast of Espírito Santo, and its formation is associated with tectonic movements that culminated in the opening of the Atlantic Ocean (Winter et al., 2007). The Albacora Field, one of the hydrocarbon exploration provinces in this basin, is located 110 km east of Cabo de São Tomé, in the state of Rio de Janeiro (Fig. 1). The hydrocarbon exploration block covers an area of approximately 455 km² and is located at the slope break, with water depths ranging from 100 to 1050 m (De Gasperi and Catuneanu, 2014).

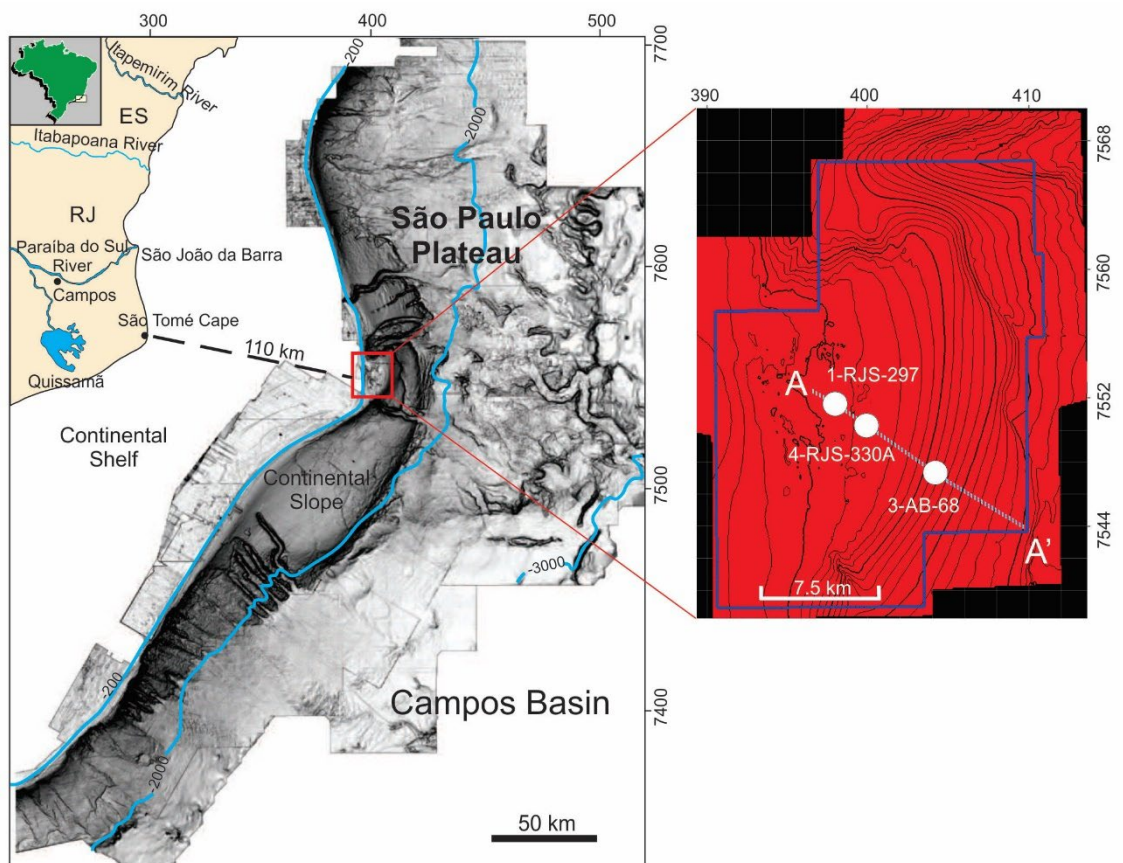


Figure 1 - São Paulo Plateau and highlighted 3D seismic survey limits with sea bottom surface and wells. The studied area is represented by 2D seismic section A -A' and wells 1-RJS-297, 4-RJS-330A and 3-AB-68 (modified from Almeida and Kowsmann, 2014).

Understanding the development of the Campos Basin is crucial for hydrocarbon exploration. For exploration and development of deposits, the subsurface modeling process includes duties such as seismic data processing and interpretation, building geological static models, and conducting dynamic fluid flow simulations (Magalhaes et al., 2020). Its architecture and evolution have been the subject of numerous studies (e.g., De Gasperi and Catuneanu, 2014; Osório, 2017; Linhares et al., 2018). Understanding the dynamics associated with slope break deposition is vital to this topic. This pertains to the stratigraphy of recently deposited sediments in the proximal portions of the basin, which are characterized by modest to moderate water depths, and the distal portions, which are characterized by significant variations in ocean depths (Menezes, 2004). This disparity results from the two systems' opposing energies. Consequently, stratigraphic studies focusing on these slope break characteristics can contribute to geohazard assessments, geomechanical analysis, and depositional models.

Another crucial point is that the zoning employed in these models, for the most part, relies on lithostratigraphy. Magalhães et al. (2020) proposed a vertical zoning approach in the geological model using high-resolution chronostratigraphy to achieve more refined results. However, conducting radiometric dating is not always feasible. Biostratigraphy assists in addressing these challenges, but it also has limitations due to the scarcity of records and the chronostratigraphic resolution it provides. One way to overcome this issue is by integrating cyclostratigraphic analysis techniques with other analytical methods, such as seismostratigraphy, biostratigraphy, and cyclostratigraphy. This integrated approach allows for the generation of high-resolution chronostratigraphic frameworks, thereby facilitating the identification and exploration of hydrocarbon deposits.

Cyclostratigraphy lets scientists look at periodic and/or quasi-periodic changes in sedimentary sequences. These changes are caused by climate forcing processes that affect the sedimentation process and are preserved in sedimentary sequences. One of its primary applications involves the identification of astronomical cycles, known as Milankovitch Cycles, whose periodicities have been reasonably well determined for the past 50 Ma. After the LASKAR 2010d (Laskar et al., 2011) solution with 405 kyr of metronome up to 250 Ma, by utilizing these cycles,

it becomes possible to achieve high-resolution temporal calibration of data series originally situated within the stratigraphic domain (Hinnov and Hilgen, 2012; Hinnov, 2013; Hinnov, 2018). Based on these factors, it can be affirmed that cyclostratigraphy plays a pivotal role in studies related to depositional processes (e.g., Locklair et al., 2008; Liu et al., 2017).

The Albacora Field (Fig. 1), located in the Campos Basin, has been under study for approximately three decades, resulting in the establishment of an extensive seismic network and a significant number of exploratory wells (Brunh et al., 2017). This provides an excellent opportunity for integrating seismostratigraphic, biostratigraphic, and cyclostratigraphic investigations in the region.

In this context, the present research focuses on the cyclostratigraphic and seismostratigraphic analysis of data obtained from three wells situated in the southern section of the Albacora Field (Fig. 1). Through the integration of these analyses with pre-existing biostratigraphic data, a 2D high-resolution chronostratigraphic model for the Miocene period in the Albacora Field is proposed.

Objectives

This master's dissertation aims to investigate the sedimentary evolution of the lower Miocene section within the Albacora Field in the Campos Basin. The primary objective is to conduct a high-resolution chronostratigraphy of the lower Miocene section, integrate existing biostratigraphic studies and cyclostratigraphic analysis, and subsequently propose an astronomical time scale (ATS) for the studied geological interval. The specific objectives of this research are as follows:

- a) Identify the periodic and quasi-periodic cycles captured in the gamma ray data from the Albacora Field by employing spectral analysis.
- b) Determine the sedimentary accumulation rates in each well and assess their variations throughout the entire sedimentary section.
- c) Validate the applicability of cyclostratigraphy methodology in a marine siliciclastic sedimentary environment at reservoir resolution.

d) Investigate the paleoclimate and paleoenvironmental changes associated with the slope break of the central-northern region of the Campos Basin.

Chapter 2

Geological Setting

The Campos Basin is a passive margin basin situated on the southeastern coast of Brazil, bounded by the Vitória High to the north and the Cabo Frio High to the south. This basin is renowned as one of the country's major oil producers. Given its significant economic importance, its tectono-sedimentary evolution has been extensively studied and documented (e.g., Asmus, 1975; Menezes, 1985; Guardado et al., 1990; Rangel et al., 1994; Winter et al., 2007).

The Campos Basin can be divided into three depositional supersequences: the rift, post-rift, and drift phases (Rangel et al., 1994; Winter et al., 2007). The rift phase is deposited on the crystalline basement of the Campos Basin, which consists of Proterozoic Ribeira Province gneisses. It is composed of the Lagoa Feia Group, which comprises the Itabapoana, Atafona, and Coqueiros Formations. The post-rift phase consists of the Itabapoana, Gargaú, Macabú, and Retiro Formations, representing evaporitic deposits. The drift phase is characterized by the deposition of the Macaé and Campos Groups. The Macaé Group is predominantly composed of carbonate sediments and includes the Goitacás, Quissamã, Outeiro, Imbetiba, and Namorado Formations. The Campos Group, the focus of this dissertation, consists of the Ubatuba (UBT), Emborê (EBR), and Carapebus Formations. The Ubatuba Formation is primarily composed of a thick sand unit known as the Siri Member (SR), with a carbonate component in the Grussai Member (GRU). The Emborê Formation is characterized by siltstones and shales of the Geribá Member (BGA), with occasional sand occurrences from the Siri Member. The Carapebus Formation is composed of shaly deposits of the Geribá Member (GBA).

The sedimentary succession under investigation comprises Miocene deposits from the Aquitanian, Langhian, and Burdigalian stages (Fig. 2). The dominant lithologies include sands deposited by dense flows and boundary currents, as well

as siltstones and shales. Within the sedimentary record, there are extensive accumulations of amalgamated sandy bodies, forming thick rock layers reaching several hundred meters in thickness. Additionally, diamictites representing portions of the slope base and deep-water marls are observed in the sedimentary sequence (Winter et al., 2017).

The Albacora Field is situated in the northern part of the Campos Basin (Fig. 1), located approximately 110 km offshore, with a water column ranging from 100 to 1050 m (De Gasperi and Catuneanu, 2014). Above the reservoir interval, the slope exhibits unique cliniform geometries, resulting in the bypass of turbidite sands and the development of diamictites and clay-rich onlap geometries within the Miocene-aged rocks (De Gasperi and Catuneanu, 2014).

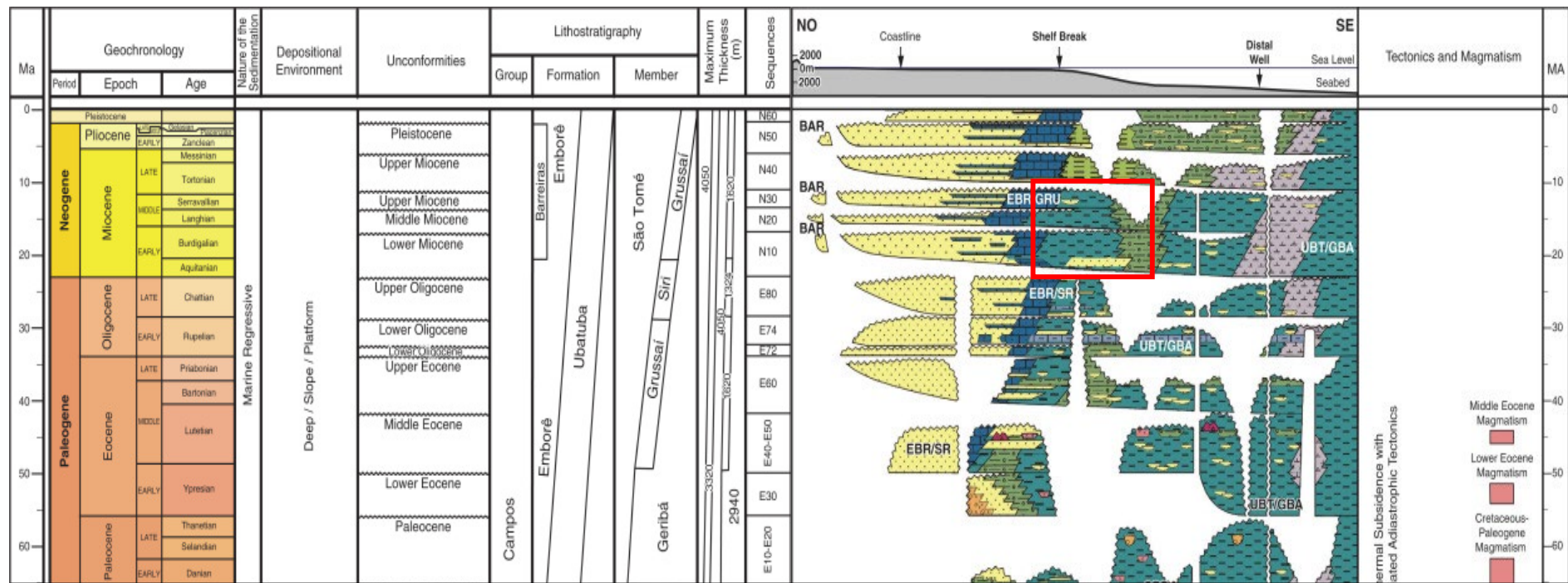


Figure 2- Campos Basin stratigraphic chart. The study marked in red square (Modified from Winter et al., 2017).

Chapter 3

Chronostratigraphy of Albacora

Terrace

Chronostratigraphy is a crucial tool for analyzing the sedimentary record as it provides detailed insights into the spatial distribution, internal variations, and overall evolution of sedimentary basins. However, the availability of radiometric dating, which is often limited due to operational factors such as costs and time, can be a challenge (Hinnov, 2013). As a result, the integration of microfossil and seismic data (allostratigraphy) along with cyclostratigraphic analysis becomes an important approach for conducting such analysis. This chapter aims to discuss the presence of chronostratigraphic information in the Albacora ring fence within the Campos Basin, which is crucial for correlating the analyzed wells in this dissertation.

The analysis of accumulated and sedimented biodiversity, along with the associated grains, provides valuable information about the deposition period of marine sediments. This field of study is known as biostratigraphy. Nannometer-sized fossils are widespread in the sedimentary basins along the Brazilian coast (Oliveira, 2004). These fossils, known as nannofossils, have been extensively utilized by the petroleum industry since the late 1960s to understand basin dynamics. They possess characteristics such as abundant occurrence, rapid evolutionary rate, wide spatial distribution, and good preservation in rocks deposited in the open ocean, such as shales and turbidites (Batiston et al., 2016). The ease of species identification and efficient processing of samples enable the dating and recognition of stratigraphic markers during well drilling, a technique known as biosteering.

The Campos Basin has been extensively studied regarding nannofossil analysis (e.g., de Oliveira, 2004; Alves, 2016; Gennari, 2018), which has provided crucial data for understanding the basin. The comprehension of the geometry and evolution of turbidite reservoirs in the Marlim and Albacora fields is an example of the contribution of these studies (Dias-Brito, 1989; De Gasperi and Catuneanu, 2014; Bruhn, 2017; Luna, 2019; Torres, 2021).

In the specific section being studied, the biozones are defined by the presence of specific taxa, namely *Sphenolithus belemnoides*, corresponding to zone N560 (18.3 – 17.95 Ma), and *Helicosphaera ampliapertura*, corresponding to zone N570 (17.95 – 14.9 Ma) (Martini, 1971; Cohen, 2013; De Gasperi and Catuneanu, 2014; Batiston et al., 2016). Figure 3 illustrates these biozones.

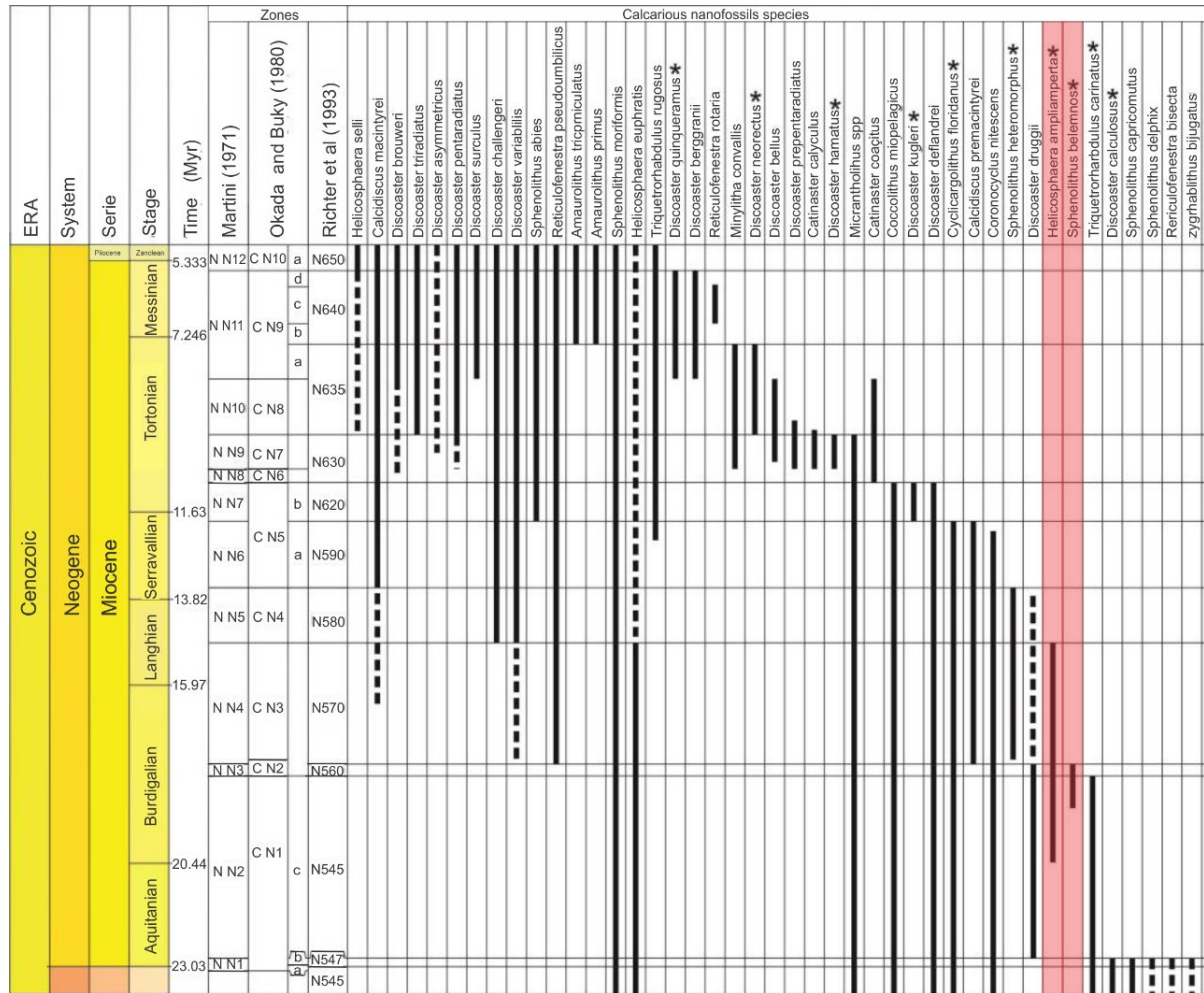


Figure 3 – Biozone distributions. The species with asterisks have their disappearances delimiting biozones in the Brazilian continental margin. Highlighted species (red rectangle) are the biozones that help tie cycles in time in study (modified from Batiston et al., 2016)

Chapter 4

Cyclostratigraphy: theoretical background

4.1 The climate spectrum

Climate variations have a significant influence on Earth's temperature, sedimentation patterns, and ultimately, the geological record (Kodama and Hinnov, 2015). For instance, during periods of reduced insolation, glaciation events can occur, leading to an Icehouse era. During such times, the sea-level drops, increasing the energy of the system and facilitating the occurrence of turbidity currents, resulting in the deposition of coarser sediment grains. Conversely, as temperatures rise, the sea-level increases, energy levels decrease, and the system becomes more quiescent, leading to the enhanced deposition of finer sediments such as clay and silt (Catuneanu, 2006).

Insolation is a crucial factor that influences climate patterns on both local and global scales, and it is determined by the amount of solar radiation received by the Earth. This radiation is regulated by the dynamic interactions within the solar system (Laskar, 1993 and 2008). These interactions, including gravitational forces exerted by other celestial bodies, contribute to the modulation of temperature cycles. For instance, when the distance between the Sun and the Earth increases, solar radiation decreases accordingly (Berger et al., 2012 and 2014).

In addition to insolation, various other variables interact and influence the Earth's climate, leading to non-linear responses and highlighting the complexity of this topic (Rial et al., 2004). These diverse factors contribute to a complex climate spectrum characterized by quasi-periodic cycles spanning a range of frequencies,

including high, medium, and low frequencies. Some examples of these cycles include daily variations (e.g., tidal cycles), sub-decadal variations (e.g., El Niño and North Atlantic Oscillation), sub-centennial cycles (e.g., Solar cycles), and millennial cycles (e.g., Heinrich events and astronomical cycles). Figure 4 illustrates some of these climate cycles.

Understanding both current and past climate cycles is crucial for comprehending the evolution of the Earth's system. Paleoclimate reconstruction serves as a vital tool in determining sedimentation rates throughout different geological periods. However, reconstructing paleoclimate has presented significant challenges for scientists over the years. Attempts to reconstruct the climate spectrum over the past 130 Ma have been made by researchers such as Mitchell (1976), Shackleton and Imbrie (1990), and Pelletier (1997). The analyzed samples encompass climate variations ranging from hourly to two hundred thousand-year timescales (Weedon, 2003).

Cycle		Time	Mechanism / Cause	
Suborbital cycles	Daily cycle	1 d.	Earth's rotation	
	Intra-season cycle	180 d.	Inclination of the Earth axis	
	Annual cycle	365 d.	Earth's translation	
	El Niño – Southern Oscillation (ENSO)	2 to 7 y.	Lunar/planetary influence	
	Schwabe cycle	11 y.	Influence of planets (Jupiter and Saturn)	
	Saros cycle	18.1 y.	Lunar orbital parameter	
	Lunar Nodal Cycle (LNC)	18.6 y.	Lunar orbital parameter	
	Hale cycle	22 y.	Influence of planets (Jupiter and Saturn)	
	Brückner cycle	35 y.	Lunar/planetary influence	
	Interdecadal Pacific oscillation (IPO)	15 to 30 y.	Lunar/planetary influence	
	North Atlantic Oscillation (NAO)	25 to 35 y.	Lunar/planetary influence	
	Pacific Decadal Oscillation (PDO)	50 to 70 y.	Lunar/planetary influence	
	Atlantic Multidecadal Oscillation (AMO)	50 to 90 y.	Lunar/planetary influence	
	Lower Gleissberg cycle	88 y.	Influence of planets (Jupiter and Saturn)	
	Upper Gleissberg cycle	120 y.	Influence of planets (Jupiter and Saturn)	
	Jose cycle	179 y.	Influence of planets (Jupiter and Saturn)	
	Suess Cycle (or De Vries Cycle)	208 y.	Influence of planets (Jupiter and Saturn)	
	500 year cycle	500 y.	Influence of planets (Jupiter and Saturn)	
	Eddy cycle	1,000 y.	Influence of planets (Jupiter and Saturn)	
	Dansgaard-Oeschger events	1,500 y.	Solar influence	
	Bond events	1,500 y.	Solar influence	
	Hallstatt cycle	2,300 y.	Influence of planets (Jupiter and Saturn)	
	Heinrich events	10 my.	Solar influence	
Orbital cycles	Milankovitch cycle	Interglacial	10 my.	Combination of orbital parameters
		Glacial	100 my.	Combination of orbital parameters
	Precession	20 my.	Orbital Parameter	
	Obliquity	40 my.	Orbital Parameter	
	Short eccentricity	100 my.	Orbital Parameter	
	Long eccentricity	400 my.	Orbital parameter	
Grand orbital cycles	Very long obliquity	1.2 My.	Gravitational interactions between the Earth and Mars	
	Very long eccentricity	2.4 My.	Gravitational interactions between the Earth and Mars	
Supercycle	Major impact event (asteroids / meteorites) or Galactic cycle	30 My.	Vertical oscillation of the Solar System perpendicular to the mid-plane of the Galaxy	

Legend: d = day(s); y = year(s); my = thousands of years; My = Millions of years.

Figure 4 - Periodicities related to the climate spectrum (Fragoso et al., 2021).

An example of a daily-scale cycle is the one induced by the dynamics of the Sun, Earth, and Moon. The astronomical tide cycle is caused by the combined gravitational forces exerted by the Moon and the Sun on the rotating Earth, which significantly influence coastal water levels (Hinnov, 2013). These periodic influences can be recorded in sedimentary deposits through changes in layer thicknesses and grain sizes, such as the intercalation of sand and mud layers. Tides

exhibit two types of cyclicity: diurnal tides and semi-diurnal tides. The diurnal tide cycle has an approximate period of 29.5 days, while the semi-diurnal tide cycle has a period of about 27.6 days (Weedon, 2005; Berger et al., 2012).

El Niño/Southern Oscillation (ENSO) is a natural phenomenon characterized by the warming of the surface waters of the South Pacific Ocean, which in turn leads to variations in the atmospheric pressure system and a decrease in the trade winds. Consequently, this phenomenon has a direct impact on the energy of the environment (Bigg, 1996; Fedorov and Philander, 2000). El Niño events occur with a cyclicity of approximately 3-5 years, and each event typically lasts for about a year. Therefore, it can be classified as a sub-decadal cycle, similar to the North Atlantic Oscillation (Fragoso et al., 2021).

The North Atlantic Oscillation (NAO) is a climatic phenomenon characterized by variations in the atmospheric pressure between the subtropical high-pressure system over the Azores and the subpolar low-pressure system near Iceland (Hurrell, 1995). The NAO influences the distribution of heat in Europe, resulting in rainfall and high temperatures in northern regions and lower temperatures in southern Europe. The NAO exhibits a frequency of variation of approximately 6 to 13 years (Weedon, 2005).

Like other climate cycles, astronomical cycles are not completely conservative or periodic, but they are considered the most regular oscillations observed in nature (Fragoso et al., 2021). As a result, cyclostratigraphic studies have utilized these cycles to obtain detailed geochronology for geological records. The topic 4.2 (Milankovitch Cycles) will provide further details on astronomical cycles.

4.2 Milankovitch Cycles

As previously mentioned, paleoclimate variations with cyclic patterns can be attributed to changes in planetary orbits resulting from dynamic and stochastic processes within the Solar System (Hinnov, 2000, 2013; Weedon, 2005; Fragoso et al., 2021). The scientist who made significant contributions to mathematically describing and relating orbital motions to these variations was Milutin Milankovitch in 1941. According to his theory, changes in astronomical parameters directly

influence the incoming and distribution of solar radiation, thereby affecting the global climate system. These cycles, known as "Milankovitch Cycles," consist of three main components: eccentricity, obliquity, and precession, which are associated with changes in the position, shape, and orientation of the Earth's orbit (Fig. 5). Additionally, the interaction between the Sun, Moon, and Earth, known as lunisolar precession, contributes to these cycles (Hinnov, 2013). Understanding these parameters forms the basis for identifying periodic and quasi-periodic variations in the geological record (Laskar, 1993; Hinnov, 2013).

The orbital cycles are a result of the changing gravitational environment as the Earth orbits the Sun (Eq. 1) (Fragoso et al., 2021; Weedon, 2003). The eccentricity of the Earth's orbit, which determines the distance between the Earth and the Sun, varies between 0.00021318 and 0.066957 (Hinnov, 2013). Currently, the eccentricity of the orbit is approximately 0.017 (Weedon, 2003). A decrease in eccentricity leads to improved Earth insolation, as shown in Equation 2. Milankovitch proposed a quasi-periodic law (Eq. 3) that indicates cycles related to this parameter ranging from ~400,000 to ~100,000 years and have remained relatively constant throughout the planet's history due to the gravitational forces exerted by the Sun and massive planets (Jupiter and Venus), which ensure their stability (Berger et al., 1992; Waltham, 2015).

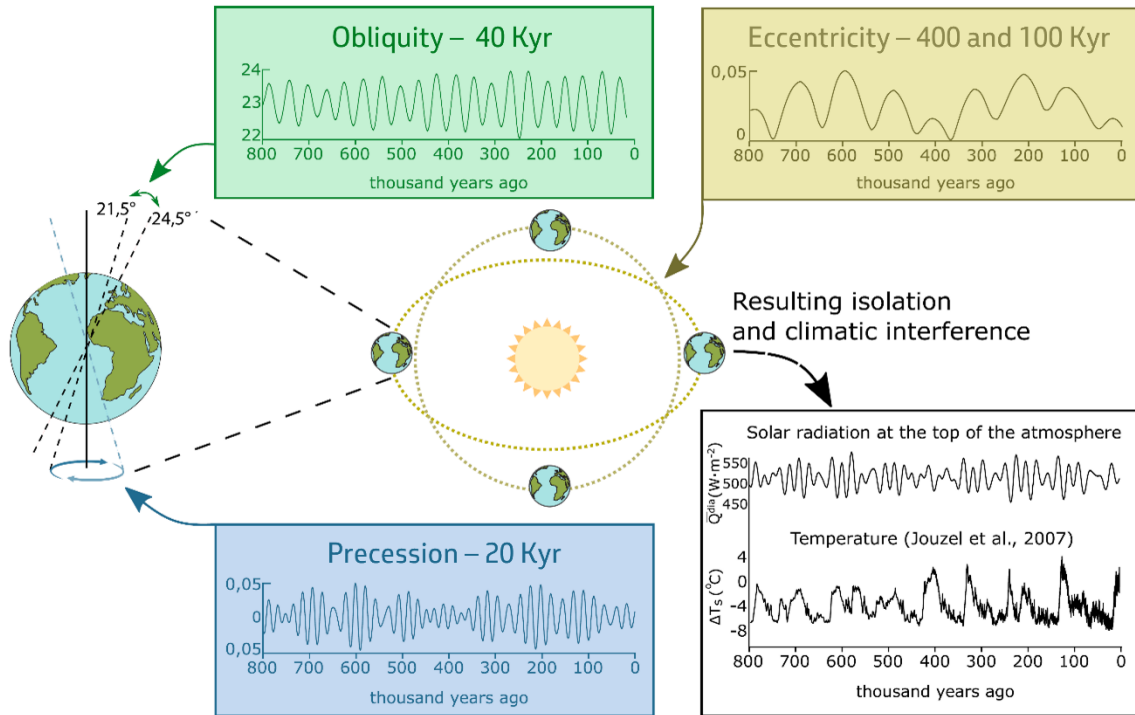


Figure 5 - Milankovitch Cycles quasi-periodicity a) Obliquity, b) Eccentricity, c) Precession and d) the result of then on insolation. (Fragoso et al., 2021).

Equation 3
$$e = \frac{(a^2 - b^2)^{1/2}}{2a}$$

Equation 2
$$W = \frac{S_0}{4(1 - e^2)^{1/2}}$$

Equation 1
$$e = e_0 + \sum E_i \cos(\lambda_i t + \phi_i)$$

Where “a” and “b” are the major and minor axis of ellipsis, “ e_0 ” is eccentricity constant that is equal 0.0287, “ E_i ” is the amplitude of the planets orbits periods, “ λ_i ” the secular frequencies of planets, “ ϕ_i ” is the constant phase, “ S_0 ” is the constant solar and “W” is the total isolation.

Lunisolar precession is the result of the gravitational interactions between the Earth, the Moon, and the Sun, leading to changes in the orientation of the Earth's rotational axis and the equatorial plane in relation to the orbital plane of the Earth around the Sun. The movement of the Moon and its gravitational influence on Earth's fluids, such as the oceans, lagoons, and rivers, creates a bulge near the equatorial

plane (Laskar et al., 2011; Hinnov et al., 2018). The Moon's orbital plane undergoes fluctuations of approximately ± 5 degrees, causing the position of the bulge to change. This, in turn, induces a torque on the solid mass of the Earth, leading to variations in the angle between the rotational axis and the equatorial plane in relation to the Sun-Earth orbital plane (Berger et al., 1992; Berger and Loutre, 1994; Hinnov et al., 2013; Waltham, 2015; Fragoso et al., 2021).

Over time, the Moon gradually moves away from the Earth, which reduces the gravitational force and mitigates the effects of the bulge. Consequently, the cycles associated with lunisolar precession, such as obliquity (tilt of the Earth's axis) and precession (change in the orientation of the Earth's axis), change over long timescales (Weedon, 2003). Obliquity refers to the variation in the inclination angle of the Earth's axis, which can range between 22° and 24.5° , with respect to a fixed reference plane (Fig. 6). The current value of obliquity is $23^\circ 27'$ (Weedon, 2003; Berger and Loutre, 2004).

Obliquity plays a significant role in the seasonal changes in insolation, resulting in shifts in heat distribution between the equator and the poles. Its influence is most noticeable at high latitudes (Hinnov, 2000). Obliquity cycles occur every 41,000 years and exhibit quasi-periodic behavior as described by Equation 4. However, obliquity has varied over geological time due to the influence of the Moon and tides on the planet's rotation (Berger et al., 1992; Waltham, 2015).

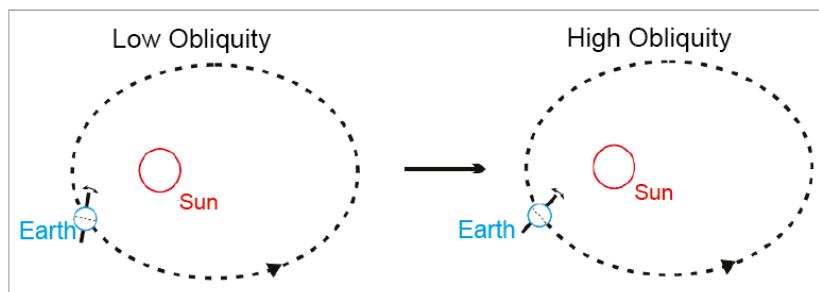


Figure 6 - Representation of the different obliquity configurations (Rodrigues, 2018).

Equation 4

$$\epsilon = \epsilon^* + \sum A_i \cos(\check{f}_i t + \check{\delta}_i)$$

Where “ ϵ^* ” is obliquity independent term that is equal 23.32, “ A_i ” is the amplitude of the planet’s obliquity periods, “ $\check{f}_i t$ ” the secular frequencies of planets obliquity, “ $\check{\delta}_i$ ” is the constant phase.

Climate precession (Fig. 7) comprises two different parameters: axial and apsidal precessions. The first is related to the “spinning top” movement of the planet caused by the gravitational force of the Moon and Sun on the equator. The apsidal precession, on the other hand, refers to the counterclockwise motion of the rotation of the semi-major axis of the Earth’s orbit (Berger and Loutre, 1994). The magnitude of the climatic precession is modulated by eccentricity in both amplitude and frequency as shown Equation 5 (Hinnov, 2000). This parameter is responsible for the characteristics of the seasons (e.g., mild summers or hot summers). The periodicity of the cycle is around 21 kyr, but since it is influenced by the Moon and tidal friction, it also varies its periodicity over the geologic past (Waltham, 2015).

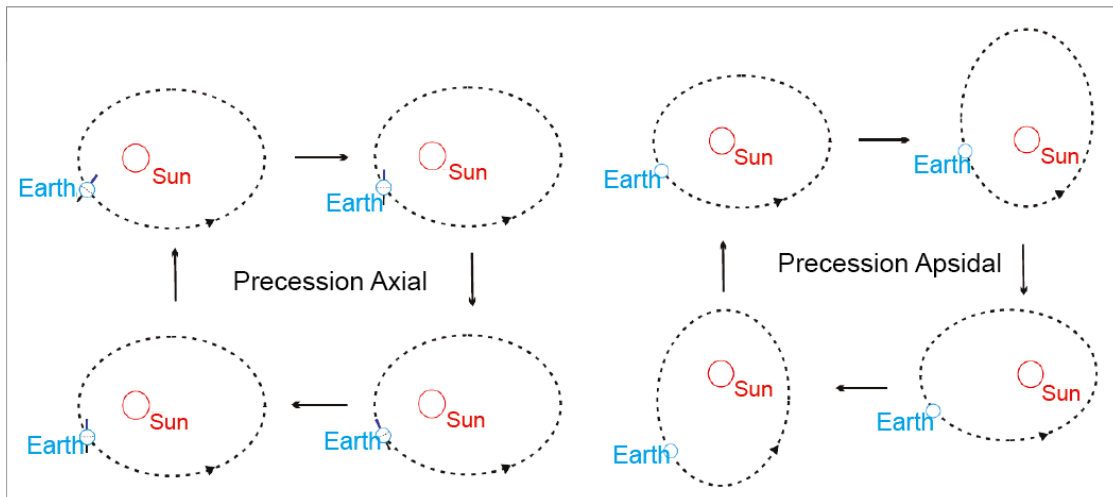


Figure 7 - Representation of the different configurations of the climatic precession. On the left the axial precession and on the right the apsidal precession (Rodrigues, 2018).

Equation 5

$$e \sin \psi = \sum P_i \sin(a_i t + \zeta_i)$$

Where “ P_i ” is the amplitude of the planet’s precession periods, “ a_i ” the secular frequencies of planets precession, “ ζ_i ” is the constant phase.

In summary, obliquity influences how solar radiation reaches the planet, while precession and eccentricity affect the distance between the Earth and the Sun. Eccentricity also plays a modulating role in obliquity and precession (Berger et al., 1992; Berger and Loutre, 1994). The recognition of Milankovitch Cycles and the analysis of paleoclimate proxies in time series allow us to observe periodic and quasi-periodic cycles in the stratigraphic record. Therefore, cyclostratigraphy aims to identify, characterize, and interpret well-established orbital cycles (Milankovitch Cycles) throughout the stratigraphic record, providing a highly accurate geochronometer for the geological past (Weedon, 2003; Hinnov, 2013).

4.3 The astronomical time scale: potential for basin chronostratigraphic frameworks astrochronology

Radioisotope dating is primarily used for older periods and is often performed on layers containing volcanic ash, although these layers are usually sparse. However, cyclostratigraphic analyses offer an alternative method to establish a highly accurate chronology for intervals that lack radiometric dating (Hinnov, 2013). The process of identifying astronomical records in sedimentary profiles involves comparing sedimentary cycles with insolation curves and astronomical models. By doing so, raw data can be converted into time series, providing valuable chronostratigraphic information throughout the geologic record. The astronomical time scale (ATS) serves as a comprehensive framework that integrates global chronostratigraphic data and is widely available for most of the Cenozoic era. Additionally, there are floating ATS for the Mesozoic era, which,

although not anchored in absolute dating, still provide valuable insights (Hinnov, 2013; Dinarès-Turell et al., 2014; Huang, 2018).

The accuracy of the results obtained through astrochronology relies on accurately identifying astronomical signals within the sedimentary record and using appropriate reference points for age adjustment (Hinnov, 2013). It is worth noting that the identification of Milankovitch Cycle wavelengths through astronomical model solutions is highly accurate for time periods up to 60 million years ago (Berger et al., 1992; Hinnov, 2018). However, for older periods, there are uncertainties in short cycles such as precession and obliquity increase due to the chaotic motions of the solar system (Laskar, 2008; Dinarès-Turell et al., 2014; Laskar et al., 2011).

In the Miocene, which is the focus of study, cyclostratigraphy has made significant contributions to various research works. For instance, Lourens et al. (2004) and Hilgen et al. (2012) conducted analyses involving biostratigraphy, magnetostratigraphy, and oxygen isotopes. These studies correlated these data with well records from the Atlantic and Pacific oceans. Zachos et al. (2001, 2008) developed an astronomical time scale for the past 35 million years based on $\delta^{18}O$ data from benthic marine organisms. In the Campos Basin, there has been limited application of the cyclostratigraphy method, with only one study conducted almost 20 years ago by Castro (2005). The author identified depositional cycles in the northern portion of the basin, that were related to eccentricity (410 and 100 kyr), obliquity (41 kyr), and precession (23 and 19 kyr) based on sonic log proxies, which are sensible to porosity and lithology. It is distinct from the gamma ray log proxy that is sensitive to granulometry, an environmental energy aspect. The concave shape of the clinofom observed in the study preserved sedimentary deposition patterns.

Chapter 5

Data and Methods

5.1 Data Acquisition

The data used in this dissertation were obtained from the National Petroleum Agency (ANP). The request for these data was made in October 2020 through the Graduate Program in Geophysics at the National Observatory. The data specifically pertain to the Albacora Field (Fig. 1) and encompass 44 exploratory wells. Additionally, the dataset includes a 3D seismic survey conducted using bottom cable acquisition with multicomponent receivers, as well as pre-stack depth migration (PSDM) processing. Furthermore, a 2D seismic campaign was carried out using streamer-type acquisition, and PSDM processing was performed on the acquired data.

The seismic data survey and well dataset were imported into the Schlumberger Petrel® 2020.3 software for correlation and seismostratigraphic interpretation (Fig. 1). Biostratigraphic information was provided by Petrobras (Petróleo Brasileiro SA) and was incorporated to assist with well correlations and serve as a temporal reference for the cyclostratigraphic analyses.

Quality control procedures were applied to the wells, including the loading of gamma ray, electrical, sonic, and density profiles. Porosity calculations were performed using the density logs to facilitate depth matching with lithologies obtained through core sampling. Velocity data from the National Agency for Petroleum, Natural Gas and Biofuels (ANP) was imported and tested with simple horizon conversion methods.

After applying the aforementioned procedures, three wells (1-RJS-297, 4-RJS-330A, and 3-AB-68) were selected for analysis in this project. It is important to note that this dissertation is part of a larger project focused on the cyclostratigraphic study of the southern and northern portions of the Albacora Field. This dissertation specifically focuses on the southern part (Fig. 1).

The selection of the wells took into consideration several factors. Firstly, wells without high-rejection faults or gas escapes were chosen. Additionally, the absence of erosive features suggests the absence of significant depositional gaps, which is crucial for conducting precise cyclostratigraphic analyses. Another important criterion for selecting the wells was their geographic arrangement within the basin. They are situated in a dip section, likely resulting in different sedimentation rates. By combining seismic interpretation with cyclostratigraphy, it was possible to analyze the continuity of these logs and observe variations in sedimentation rates among the wells.

5.2 Seismic Interpretation

Typically, seismic processed data consists of seismic traces (1D), a set of seismic traces in a line (2D seismic), or a set of lines (3D). The interpretation of this data aims to generate a geologic model of the subsurface (Bruhn et al., 2017; Linhares et al., 2018; Fonseca et al., 2018). Seismic reflections carry chronostratigraphic significance as they represent synchronous timelines. Picking horizons of negative, positive values, or zero-crossings is done to provide a geometric representation of the stratigraphy and, subsequently, a representation of geologic time (De Gasperi and Catuneanu, 2014; Catuneanu, 2016).

Otherwise, the seismic interpretation of the 3D data is applied in four distinct steps: 1) horizon mapping in time, 2) velocity modeling, 3) study of seismic resolution, and 4) seismic attribute analysis. The cyclostratigraphic correlation requires the outputs of the first three steps. Steps 1 and 2 are necessary to convert the seismic horizons to depth and enable stratigraphic correlation between the wells.

The velocity model (step 3) establishes a reliable relationship between seismic depth and well depth since the seismic data is in time depth. Seismic amplitude data has a lower frequency and thus a resolution of meters, whereas well logs have a higher resolution of centimeters. Therefore, a resolution study is necessary to determine the range of the seismic horizon's position in terms of well depth (Widess, 1973).

Creating or calibrating the time/depth relationship is an important step in the seismic interpretation process (Maul et al., 2021). There are three types of velocities: 1) root mean square (RMS) velocity, 2) interval velocity, and 3) average velocity (Fonseca et al., 2018). The first two are used in processing seismic data (migration and stack steps), while the average velocity is crucial for converting time to depth. Amaral et al. (2015) presented a robust workflow for generating a velocity model. The methodology consists of the following steps: 1) calculating the interval velocity from sonic log data in a well to establish an initial time/depth relationship, 2) correlating the well with seismic data and re-calculating the velocity, 3) deriving the average velocity from the interval velocity, and 4) establishing three additional relationships through extrapolation using external drift.

5.3 Cyclostratigraphy Analysis

Cyclostratigraphy is a branch of sequence stratigraphy that aims to identify and interpret periodic and quasi-periodic cycles in stratigraphic records (Weedon, 2003). Sedimentary deposits have the potential to contain valuable information about climatic cycles. To identify these cycles, it is important to consider the variations in accumulation rates within different depositional environments. When these rates are consistently low and there is continuous sedimentary deposition without significant gaps, there is a higher likelihood of preserving the record of periodic or quasi-periodic paleoclimatic variations. These variations manifest as changes in the physicochemical properties of the deposit. Therefore, faciological analyses, geochemical data, magnetic mineralogy data, and well logging techniques can be employed to identify and analyze these changes (Hinnov, 2013). The workflow for conducting this type of analysis can be found in Figure 8.

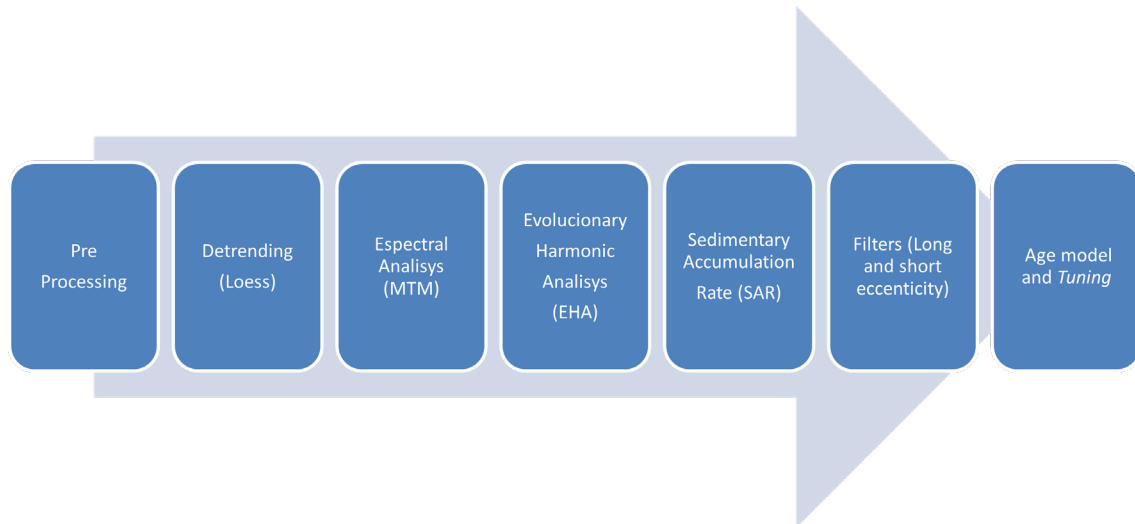


Figure 8 - Cyclostratigraphic analysis workflow.

5.3.1 Time-series Analysis

The utilization of spectral estimation is a method employed to identify periodic and quasi-periodic patterns inside the frequency domain (Laskar et al., 1993; Hinnov, 2013, 2018). Through the identification of these cyclical signals, it becomes feasible to establish a correlation between distinct time spans and the geological record. There exist multiple techniques that can be utilized for the computation of harmonic signal components. Among these techniques, the periodogram is frequently utilized in the field of cyclostratigraphic investigations. Nevertheless, alternative approaches exist and will be examined in subsequent sections.

The periodogram is a well-defined technique utilized for the estimation of frequency spectra (Weedon, 2003). The discrete Fourier transform (DFT) is employed to acquire it, utilizing mathematical techniques. The Fourier transform facilitates the processing of a time series by converting it from the temporal domain to the spectral domain. It is important to exercise caution when employing the periodogram for time series that possess continuous spectra, unless the underlying background is indicative of white noise (Percival and Walden, 1993). White noise refers to a random noise that is uniformly distributed over all frequencies of the data.

Sum the results and multiply them by a constant ($2/N$, where N is the number of data points) (Equation 6). This results in the average amplitude of the cosine component at that frequency. The sum is then multiplied by a sine wave of the same frequency, and the products are once again added and multiplied by a constant. For each examined frequency, the average phase of the time series oscillations is determined by the relative magnitude of the average sine and cosine amplitudes. At the desired frequency, the periodogram is produced by adding the root mean squares of the sinusoidal and cosine amplitudes. The periodogram is produced by the power plot (or root mean square amplitude) versus frequency (Weedon, 2003).

Equation 6
$$x_k = \sum_{n=0}^{N-1} x_n \left(\cos \frac{2\pi kn}{N} - i \sin \frac{2\pi kn}{N} \right)$$

Where x_k is the frequency of all data and x_n is the amplitude of each frequency that compound the periodic equation.

The Multipaper or Thomson Tapering Method (MTM) is a computational technique that relies on the periodogram. The method established by Thomson (1982, 1990) entails the summation of a limited number of tapers characterized by distinct frequency bandwidths. The aforementioned tapers, referred to as discrete spheroidal sequences or Slepian sequences, are specifically engineered to adjust the characteristics of time series data. The use of the multitaper method (MTM) has been found to be helpful in mitigating spectral leakage originating from the main lobe. Additionally, it has been observed to reduce bias, preserve frequency resolution, and improve statistical stability (Candy, 1988, 2019). In the analysis, it is customary to employ a range of one to eight tapers. Following the application of each taper on the data, a spectrogram is formed as described by Kodama and Hinnov (2015). The multitaper method (MTM) has been found to enhance the degrees of freedom and exhibit greater computational efficiency, with about double the number of tapers, in comparison to the periodogram as discussed by Percival and Walden (1993). As a result of these benefits, the utilization of MTM is prevalent in the field of cyclostratigraphy.

5.3.2 Evolutionary Harmonic

Analysis

In signal interpretation, the power spectra and frequency content can vary in space or time, especially in deep-water fields where thousands of rock property samples are available (Bruhn et al., 2017; Fonseca et al., 2018; Li et al., 2019). Analyzing these numerous samples of the proxy requires analyzing the contribution of depth converted to time on the periodogram.

Evolutionary harmonic analysis (EHA) involves creating a 3D cross-plot of the MTM spectrum (Thomson, 1982, 1990) or Fast Fourier Transform (FFT) spectrum (Kodama and Hinnov, 2015) with depth. EHA estimates the frequency content of a proxy within a depth/time sliding window (Kodama and Hinnov, 2015; Hinnov, 2016; Candy, 2019), providing both global and localized analyses of signal behavior and sedimentation rate across the well (Hinnov, 2016). In EHA, the window size is crucial because if the window is too short, it may not accurately estimate long cycles (e.g., eccentricity and obliquity), whereas if the window is too long, high frequencies will be suppressed in the cross-plot (Li et al., 2019).

5.3.2 Filters and Astronomical

Tuning

An astronomical solution used in cyclostratigraphy is the insolation model, which relies on the estimation of Milankovitch cycles (Milankovitch et al., 1941; Berger et al., 1992; Laska et al., 2004; Laskar et al., 2011) based on astronomical records and planetary ephemeris data. The Laskar solutions (Laskar et al., 2004; Laskar et al., 2011) are astronomical models that describe the Milankovitch cycles using secular frequencies of precession denoted as "g_i" and "s_i," along with a precession constant "k" (Eq. 7). The index "i" corresponds to the number of the planet (e.g., 1 = Mercury, 2 = Venus, 3 = Earth, 4 = Mars, 5 = Jupiter, 6 = Saturn, 7 =

Neptune, and 8 = Uranus). Some cycles, such as the g2-g5 cycle (405 kyr), are related to eccentricity.

$$\text{Equation 7} \quad k = \frac{3}{2} \frac{n^2}{\omega} \frac{C-A}{c} [(1 - e^2)^{-1.5} + \frac{m_c}{m_\odot} \frac{a^3}{a_c^3} (1 - e_c^2)^{1.5} \left(1 - \frac{3}{2} \sin^2 i_c\right)] \cos h$$

Where “n” is the mean motion of the Sun in a geocentric reference frame, “ ω ” is the rotational angular velocity of the Earth, “A” and “C” are Earth's moments of inertia around the equatorial and polar principal, a_c and e_c is semi-major axis and eccentricity of the Moon's orbit around the Earth, “ m_c ” is mass of the Moon, “ m_\odot ” is mass of the Sun, “ i_c ” is inclination of the lunar orbit regarding the ecliptic plan and h is constant value equal 23.40° (Hinnov et al., 2018). The precession constant is the term that respond for lunisolar precession, then change with time. For Laskar models the Milankovitch cycles is represent by table 1 (Laskar et al., 2011).

Table 1 - Main frequencies and periods index over 0-4Ma (Modified from Hinnov et al., 2013)

Term	Frequency (arcsec/yr)	Period (k.y.)
<i>Obliquity</i>		
k+s₃	31.6132	40.996
k+s₄	32.6799	39.657
k+s₃+g₄-g₃	32.1827	40.270
k+s₆	24.1277	53.714
k+s₃-g₄+g₃	44.8609	28.889
<i>Precession index</i>		
k+g₅	54.7064	23.690
k+g₂	57.8949	22.385
k+g₄	68.3691	18.956
k+g₃	67.8626	19.097
k+g₁	56.0707	23.114
<i>Orbital Eccentricity</i>		
g₂-g₅	3.1906	406.182
g₄-g₅	13.6665	94.830
g₄-g₂	10.4615	123.882
g₃-g₅	13.1430	98.607
g₃-g₂	9.9677	130.019

To distinguish the contributions of each Milankovitch cycle in the sedimentary record, it is necessary to filter the data series. The initial filtering step involves detrending the data. Many data sets exhibit trends such as overburden effects or long-term secular trends, which can obscure the quasi-periodic cycles or the target cycles of interest. To isolate the frequencies associated with the Milankovitch cycles, a detrending filter is applied. This mathematical operation involves estimating a function (e.g., linear, loess) and subtracting it from the data. Loess, for example, is a weighted moving average that estimates a cycle by smoothing a window within the data. This process helps reveal the cycles within the selected window (Kodama and Hinnov, 2015).

After identifying sedimentary cycles through time series analysis and EHA, a crucial step in cyclostratigraphic studies is to correlate these sedimentary frequencies with astronomical cycles such as eccentricity (e.g., 410/405 kyr, 125 kyr, and 100/95 kyr), obliquity (e.g., 41 kyr), and precession (e.g., 21 kyr and 19 kyr) using the astronomical solutions provided by Berger et al. (1992), Berger and Loutre (1994), Dinarès-Turell et al. (2014), and Hinnov and Hilgen (2012). Frequency filters are employed to aid in the astronomical tuning process. Low-pass filters isolate low-frequency components and facilitate the tuning of long cycles such as eccentricity and obliquity. High-pass filters isolate high-frequency components and assist in tuning short Milankovitch cycles, such as precession. Pass-band filters can be used to focus on specific Milankovitch cycles (Kodama and Hinnov, 2015; Li et al., 2019).

The process of astronomical tuning aims to identify the astronomical solution that shows the strongest correlation coefficient between the paleoclimate data series and the sedimentation rate within the stratigraphic framework. This step allows for the transformation of the analyzed data into a high-resolution dating method, facilitating the construction of an astronomical time scale that is specific to the study region (Dinarès-Turell et al., 2014).

The techniques used for astronomical tuning include visual tuning, correlation coefficient (eCOCO), and the TimeOpt Approach (Meyers and Sageman, 2007; Meyers et al., 2012; Meyers, 2015). Visual tuning involves visually comparing the filtered data with the filtered astronomical solution to adjust the amplitudes of peaks, troughs, and crossings (Weedon, 2003; Hinnov, 2012). COCO (Correlation Coefficient) uses the power spectra of the proxy data and correlates the frequency band ratios with the astronomical solution (Li et al., 2018). The evolutionary correlation coefficient (eCOCO) is applied by sliding a window sample-by-sample at depth to estimate a 3D cross-plot of sedimentation rate, depth, and COCO. The TimeOpt Approach employs Monte Carlo simulations developed by Meyers (2015) to fit the data to the astronomical solution, utilizing precession sedimentation rates modulated by eccentricity or precession. Prior interpretation using periodogram and EHA is crucial for this method. In this work, the main technique employed is

visual tuning, while COCO and eCOCO are used as a double check with the sedimentation rates of the area.

Chapter 6

About the manuscript “INTEGRATION OF SEISMIC AND CYCLOSTRATIGRAPHY FOR HIGH RESOLUTION CHRONOSTRATIGRAPHIC CORRELATION: THE ALBACORA RING FENCE, CAMPOS BASIN, BRAZIL”

The results of this master's degree dissertation have been submitted as a paper to the peer-reviewed journal Marine and Petroleum Geology (refer to chapter 7). The paper focuses on the correlation of three wells and the establishment of age-based zones using astronomical forcing theory and the integration of seismic horizons. A resolution study was conducted on the seismic data to assess the limitations of tying horizons to Milankovitch cycles. This approach is significant as it demonstrates the robustness of the dating method and addresses the challenge of integrating two geophysical methods with different resolutions while accounting for seismic uncertainties.

Chapter 7

INTEGRATION OF SEISMIC AND CYCLOSTRATIGRAPHY FOR HIGH RESOLUTION CHRONOSTRATIGRAPHIC CORRELATION: THE ALBACORA FIELD, CAMPOS BASIN, BRAZIL

Natália Braun dos Santos^{1*}, Ciro Climaco Rodrigues^{1,2}, Daniel Ribeiro Franco¹, Mingsong Li³, Mariana Aragão Fernandes¹, Mariane Candido¹, Raysa de Magalhães Rocha¹, Thiago Pereira dos Santos⁴, André De Gasperi², Daniel Galvão Carnier Fragoso^{2,5}, Gabriella Fazio⁶, Ana Natália Gomes Rodrigues²

¹ Departamento de Geofísica, Observatório Nacional, Rio de Janeiro, Brazil;

² Petrobras, Rio de Janeiro Brazil;

³ Key Laboratory of Orogenic Belts and Crustal Evolution, MOE, School of Earth and Space Sciences, Peking University, Beijing, China;

⁴ School of Arts, Sciences and Humanities, University of São Paulo, São Paulo, Brazil;

⁵ Instituto de Geociências, Universidade Federal do Rio Grande do Sul, Porto Alegre, Brazil;

⁶ Instituto de Geociências, Universidade de Brasília, Brasília, Brazil.

Keywords: (6) orbital tuning; gamma ray log; Miocene Optimum Climate; paleoclimate; Milankovitch Cycles.

ABSTRACT

High-resolution chronostratigraphy is fundamental for a refined interpretation of the evolution of sedimentary basins and, consequently, for generating more accurate geological models, which are essential for oil and gas exploration. This study provided an innovative integration of seismic reflectors interpretation, a biostratigraphic framework and 405-kyr astronomically-tuned age models from three wells, arranged in a dip section comprising Miocene deposits in the slope break of the Albacora Field, Campos Basin, Brazil. We (i) to provide a high-resolution, 2D astrochronologic model from the combination of three astronomical timescales (ATs) – comprising a timespan of ~3 Myr for the dip section; (ii) infer that the studied section comprises the middle Miocene deposits and records the Miocene Optimum Climate, and the significant eustatic falls that delimit this event; and (iii) provide refined age estimates for the seismic reflectors near the biozones.

1. INTRODUCTION

In the last decades, the orbitally-calibrated cyclostratigraphy has been considerably useful in improving the temporal resolution of the geological time scale, as well as to provide new subsidies about past sedimentary processes and its rates. Cyclostratigraphic analyses are based on the recognition of multimillennial-scale (104–106 yr), quasi-periodic Milankovitch imprint in climate-sensitive sedimentary records. When tuned to astronomical target curves given by accurate models of Earth's orbital-rotational behavior, cyclostratigraphic records of orbitally-forced climate change provide an unprecedented, high-resolution geological time scale - the astronomical time scale

(ATS) - at least as far as back to 50 Ma due to the uncertainties in the theoretical astronomical solutions (Berger et al., 1992; Hinnov and Hilgen, 2012; Hinnov, 2013; Wu et al., 2013; Meyers, 2019). For periods back to 50 Ma, the 405-kyr long eccentricity cycle (which is the expression of orbital perihelia of Venus and Jupiter and considered as quite stable over geological times) has been successfully employed for astronomical calibration even for Mesozoic deposits (Kent et al., 2018; Meyers, 2019; Leandro et al., 2022).

Chronostratigraphic investigations solely based on radiometric dating and biostratigraphy usually present limitations due to the common impossibility of obtaining datable materials and pitfalls on identifying biozones with restricted distribution and resolution (e.g., Miller, 2006; Delabroye and Vecoli, 2010; Joshi et al., 2021). Therefore, cyclostratigraphic analysis has been increasingly employed in the hydrocarbon exploration and production sectors due to the rising demand for more refined chronostratigraphic frameworks and new information on the basin's depositional dynamics (e.g., Mattner and Al-Husserini, 2002; Behdad, 2019; Makled, 2021). For instance, Falahatkah et al. (2021) investigated the control of orbital forcing on facies distribution and their associated hydrocarbon reserves in the Asmari Formation (southwestern Iran), deposited during the Oligocene-Early Miocene. By recognizing eccentricity cycles of 405 kyr in the studied wells, they identified the time interval of formation deposition and determined that it was influenced by Milankovitch-driven eustatic sea level changes. Fang et al. (2023) presented a novel approach to understanding the relationship between lithofacies and astronomical cycles in predicting favorable lithofacies for shale oil exploration in continental rift basins, using lacustrine shales from the Eocene Shahejie Formation (China). The periodic changes in long eccentricity, obliquity, and precession formed different scales of lithofacies cycles, which were

evidently controlled by paleoclimate, and a new model of shale deposition was established. In order to date and calibrate the depositional sequences of the Aquitanian-Burdigalian depositional sequences, Farouk et al. (2022) constructed a gamma-ray (GR)-based ATS for the Jambour Oil Field, Iran. The authors found a strong correlation between the astronomical solution of Laskar et al. (2011) and the current data, and the cyclostratigraphic analysis compared with global events validated the high-resolution tuning merged by eccentricity cycles. In such context, the Albacora Field, located in the north-central portion of the Campos Basin - one of the largest oil-producing basins along the passive margin of Brazil (Dias et al., 1990; De Castro and Picolini, 2015) - has been intensively studied due to its economic importance for the last 30 years. A large amount of seismic data, well-log data and biostratigraphic evaluation is already available for the Albacora Field (e.g., Asmus, 1975; Menezes, 1985; Guardado et al., 1990; Rangel et al., 1994; Winter et al., 2007; Bruhn et al., 2017). Therefore, it is a suitable target for an integrative study comprising seismic reflector and biostratigraphic framework interpretations together with individual, one-dimensional (1D) ATSS provided from chosen wells, aiming to provide a high-resolution, 2D astrochronology model for the southern Albacora Field. Such effort could provide new subsidies on the basin's depositional evolution and new geological models, of importance for optimizing the oil and natural gas exploration and production at the Campos Basin (Magalhães et al., 2020).

2. GEOLOGICAL SETTING

2.1 Campos Basin

The Campos Basin (Southeast Brazilian continental margin) - one of the most important offshore Brazilian hydrocarbon provinces - is a passive margin basin limited, respectively, to the north and south by the Victoria-Trindade Chain and Cabo Frio arch.

Since the 1970's its tectono-sedimentary evolution has been intensively studied and described due to its economic importance (e.g., Asmus, 1975; Menezes, 1985; Dias et al., 1990; Guardado et al., 1990; Dias et al., 1990; Rangel et al., 1994; Winter et al., 2007). The onset of Campos Basin dates back from the Early Cretaceous during the Mesozoic Gondwanaland break-up (Contreras et al., 2010). It has been subdivided into three major tectono-sedimentary mega-sequences or units: (1) rift sequence; (2) transitional or initial drift sequence; and (3) passive margin or final drift sequence (Rangel et al., 1994; Winter et al., 2007; Castro and Picolini, 2015). The rift phase is associated with a non-marine sequence and was deposited on the crystalline basement of the Campos Basin. The transitional phase is associated with marine and continental sedimentation and represents the lacustrine carbonates and evaporitic deposits. The final drift phase is formed by a marine sequence controlled by crustal thermal subsidence and halokinetic movements. This last stage occurred between the Aptian/early Albian to the Holocene, and is represented by the deposition of the Maca'e and Campos Groups. Carbonatic sediments dominate the Maca'e Group, whereas the Campos Group is predominantly siliciclastic (Winter et al., 2007). This last phase, which comprises our study area (Miocene deposits of the Albacora Field), is a 1st order sequence and corresponds to the divergent continental margin (passive margin) (De Gasperi and Catuneanu, 2014). Sedimentation in the Campos Basin has been controlled by the interaction between morphology (slope break), bottom currents, and sediment supply (Viana, 2001) since the Neogene until the present. Depositional rates have increased mainly due to the tectonic reactivation that resulted in the formation of the Serra do Mar Mountains in the Eocene (Cogn'e et al., 2011, 2012). The Albacora Field reservoir is located in the north-central portion of the Campos Basin (Fig. 1), approximately 110 km from the coast (De Gasperi and Catuneanu, 2014). The sedimentary package investigated corresponds to the Miocene sediments of

the Aquitanian, Langhian and Burdigalian stages. The Albacora ring fence, exploratory block, is approximately 455 km² and lies on the slope break in a water column ranging from 100 to 1050 m (De Gasperi and Catuneanu, 2014).

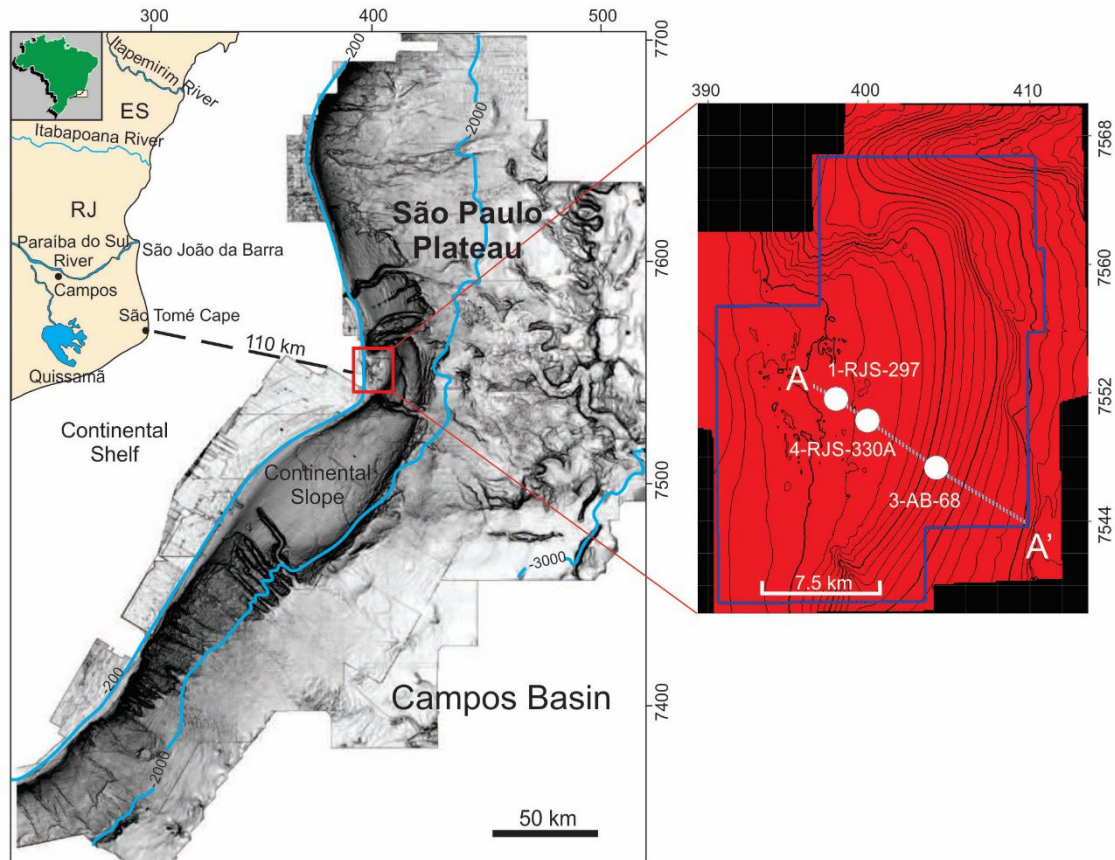


Figure 1 - Left: Bathymetric and geomorphic map of the Campos Basin highlighting the location of the study area; right: 3D bathymetric map of the studied area, wells and the limitation (ring fence) of Albacora field (blue polygon). The studied area is represented by seismic section A -A' and wells 1-RJS-297, 4-RJS-330A and 3-AB-68 (Modified from Almeida and Kowsmann, 2014).

2.2 Wells 1-RJS-297, 4-RJS-330A and 3-AB-68 (southern portion of Albacora ring fence)

Our study area is located in the slope break at the southern portion of the Albacora Field (Fig. 1). Due to the absence of significant erosional surfaces and major tectonic faults revealed by seismic interpretation, three wells in the dip section were selected: wells 1-RJS-297 (landward portion), 4-RJS-330A (central portion) and 3-AB-68 (farther offshore). They are associated with water columns of 280 m, 313 m, and 652 m, respectively, and with the following spatial distribution at the A-A' dip section: 2384 m (wells 1-RJS-297 and 4-RJS-330A) and 4939 m (wells 4-RJS-330A and 3-AB-68) (Fig. 2).

Two biozones (CN4/CN3 and CN3/CN2; Okada and Bukry, 1980; Castro, 2005; Batiston et al., 2016) were identified in well 1-RJS-297 at depths of 1540 m and 2370 m and were considered in this study as tie-points (Fig. 2). This record represents the assemblages *Helicosphaera ampliaperta* and *Sphenolithus belemnos* which exhibit associated extinction ages of 14.90 and 17.95 Ma, respectively (Okada and Bukry, 1980; Gradstein et al., 2018). Lithostratigraphic information for the three wells indicates intercalation of marl and shale with some sandstone layers. According to Mutti and Carminatti (2012) and Pandolpho et al. (2021), these layers represent deposits formed by a mixture of turbidite-contourite systems due to their location on the edge of the platform. According to Pandolpho et al. (2021), the turbidite-contourite sequence was formed

during the middle Miocene due to a drop in sea-level.

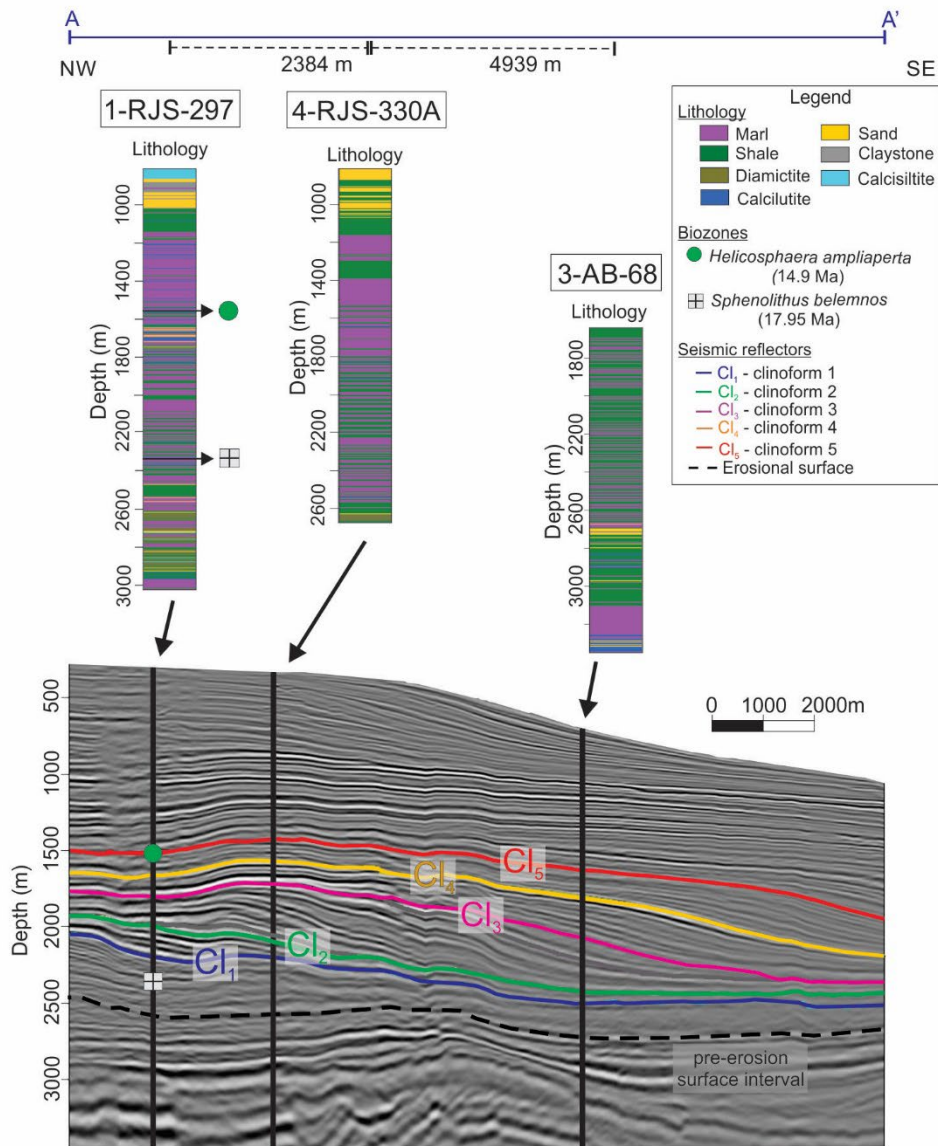


Figure 2 - Interpretation of 2D seismic section with seismic horizons, logs lithology and biozones.

The Continuous color lines are the clinoforms in the analyzed GR dataset; and the black dashed line is the erosional surface. See Figure 1 for seismic section (A-A') and location of wells.

3. DATA AND METHODS

3.1 Well-logging and gamma-ray datasets, 3D seismic lines

Well-logging data and 3D seismic lines were provided for this study by the Brazilian National Agency for Petroleum, Natural Gas and Biofuels (ANP). The seismic data was required in order to choose adequate wells for this research (without tectonic faults, gas escape, and significant erosional surfaces) and to support the wells correlation for constructing the 2D cyclostratigraphy model.

Gamma ray (GR) datasets were considered as a proxy for this study, which were taken with an average sampling rate of 0.20 m. This proxy indicates the presence of clay minerals and organic matter, reflecting paleoclimatic conditions (Li et al., 2019a; Ruffel and Worden, 2000). Thus, variations in the values of this parameter denote changes in terrestrial weathering as well as physical/chemical variations in oceanographic parameters (Li et al., 2019a). GR data has been widely used in astronomical signal extraction in sedimentary records due to their fast and easy retrieval, and excellent response to planetary climate variations (e.g., Baumgarten and Wonik, 2015; Li et al., 2019a; Gong, 2021).

3.2 Seismic Interpretation

Seismic, biostratigraphy, and well logging datasets were loaded into the French-American Schlumberger Petrel® 2020.3 software. Previous research by De Gasperi and Catuneanu (2014) presented a 3D seismostratigraphic study for the same area. The mapping of the seismic horizons was performed with Petrel software with the data in time. After mapping, we densified the 3D seismic interpretation based on the work of De Gasperi and Catuneanu (2014), which went from 50×50 to 10×10 crosslines. It allowed us to generate a surface by interpolation that was more faithful to the area's geology, as well as to enable the velocity model recalibration of the ANP data pack, reducing depth

errors. Since no seismic lines cross the selected wells for the cyclostratigraphic analysis, it was necessary to generate a 2D section from the interpolation of the 3D seismic data. We used this section to identify clinoforms and erosional surfaces for the correlation with the cyclostratigraphic data. The velocity model and the 2D section allowed a robust correlation between seismic horizon depths and wells. Additionally, a seismic resolution study (Widess, 1973) was conducted in order to (i) obtain an even more accurate fit between the depths of the seismic horizons; (ii) estimate depth uncertainties and hence enabling a reallocation of the seismic horizons in the wells; and (iii) evaluate the displacement of seismic reflectors for the procedures of astronomical tuning, when two or more clinoforms can be used to transpose the tie-points. It is critical, as the displacement of reflectors would directly influence which cyclic bundlings would be chosen to perform tuning and to generate the ATS. The resolution evaluation for the seismic reflector yielded 30 m, which means they can be displaced 15 m above or below their original position.

3.3 Cyclostratigraphy analyses

Cyclostratigraphic analyses for GR data from the three wells were performed by using Acycle version 2.4.1 software (Li et al., 2019b). Fig. 1 shows the location of the three analyzed wells. All GR series have been processed to remove the null values and then interpolated by 0.2 m to obtain a constant spacing between samples, prior to a detrending procedure by applying LOESS regression with a 400 m window. Such approach is necessary to remove irregular and low-amplitude frequencies, which correspond to very-long wavelengths not directly related to orbital variation (Weedon, 2003; Kodama and Hinnov, 2015; Li et al., 2019b).

Spectral analyses were carried out with a multi-taper spectral estimator (MTM) to identify the most significant frequencies above 90%, 95%, 99%, and 99.9% confidence

levels (Thomson, 1982). The MTM was performed with two 2π tapers and the robust first-order autoregressive AR (1) model (Mann and Lees, 1996). In order to track the changes in orbital cycles generated by the variations in sedimentation rates, the evolutionary harmonic analysis (EHA) was performed by the Fast Fourier method (eFFT) with a 250 m moving window (Kodama and Hinnov, 2015). From these analyses, we identify the bands related to the Milankovitch cycles using the ratios of the frequencies for the Miocene (mean age of 17 Ma). The ratio of the orbital frequencies was assumed to be approximately $405:125:95:40.6:23.5:18.8 = 21.46:6.62:5.03:2.15: 1.25:1$ (Laskar et al., 2011). In order to isolate the long and short eccentricity frequencies, we used the Acycle's Gaussian bandpass filtering tool. We compared these filters with Laskar et al., 2011 astronomical model (Laskar et al., 2011) for astronomical adjustment (tuning) of each of the wells and for constructing the anchored ATS.

Additionally, we investigated the optimal sedimentation rate and the null hypothesis of no orbital forcing (H_0) based on our astrochronological interpretation by performing the correlation coefficient (COCO) and evolutionary correlation coefficient (eCOCO) analyses (Li et al., 2018a). It was conducted by running 2000 Monte Carlo simulations, with the sedimentation rate ranging from 0 to 100 cm/kyr, and applying a classical AR (1) and the remove red noise. The moving window used for our eCOCO analysis was set to 250 m.

4. RESULTS

4.1 Preliminary chronostratigraphy framework: biostratigraphy and seismic interpretation

Identifying reflectors and time-to-depth migration in the 2D seismic section provided the correlation between the studied three wells. We used the seismic interpretation to identify clinoforms and the erosional surface found at the depths where

the astronomical investigation was performed. The erosional surface was determined by using reflector truncation and chaotic facies. The clinoforms have morphologies ranging from sigmoidal, flat, and convex and are identified in Fig. 2.

Two tie-points were considered for well 1-RJS-297, based on the extinction ages of the taxa *Helicosphaera ampliaperta* and *Sphenolithus belemnos* (14.9 and 17.95 Ma, respectively; Okada and Bukry, 1980; Gradstein et al., 2018). The closest clinoforms to these biozones are CL1 and CL5, respectively (Fig. 2). Clinoform CL5 is located at the same depth (1540 m) as the *Helicosphaera ampliaperta* species and, therefore, the age of 14.9 Ma was associated with it. Clinoform CL1 is located at ~180 m from the *Sphenolithus belemnos* species, and does not have a direct correspondence with the age of this biozone.

Regarding biostratigraphic information is only available for well 1- RJS-297, but both three wells are within the same geological context in local scale and sharing the same seismic expressions, we performed the following set of procedures: (i) we provided age estimates for specific clinoforms for well 1-RJS-297 by means of its anchored ATS; (ii) it was assumed the same age estimates for these clinoforms at wells 4-RJS- 330A and 3- AB-68; and (iii) floating ATSs for wells 4-RJS-330A and 3- AB-68 were anchored in time by the clinoforms (and its associated ages). The numbered clinoforms (CL1, CL2 ...) in the dataset utilized in the cyclostratigraphic analyses were then used to gauge the number of astronomical cycles between the wells.

4.2 Cyclostratigraphy

4.21 Time-series analysis

For the three wells, the 2π MTM spectral analysis of the GR data revealed peaks with statistically significant values above 95% confidence. The joint MTM and EHA

analyses allowed for the tracking and identification of the bands representing the long (E) and short (e) eccentricity, obliquity (O), and precession (P1 and P2) cycles (Figs. 3–5).

For well 1-RJS-297, the ratios used for astronomical cycles in the Miocene and their corresponding central wavelengths were $150.5:58.2:36.8:17.4:9.6:7 = 21.5:8.31:5.25:2.48:1.37:1$. The eFFT shows stability along the stratigraphic column for the long eccentricity cycle (E). In contrast, other cycles, with higher frequencies, have a representative drop in signal at depths above ~1200 m and below ~2450 m (Fig. 3c). For well 4-RJS-330A, the identified cycles in the 2π MTM spectral analysis obeyed the central wavelength ratio of $165.4:57.1:37.1:15.1:9.2:7.3 = 22.65:7.8:5.08:2.05:1.26:1$. We were able to trace the cycles along the depth with the combined analysis of the spectral peaks with the eFFT results (Fig. 4c). In well 1-RJS-297, there is a drop in signal in the short eccentricity, obliquity, and precession cycles between depths above ~1200 m and below ~2450 m. Well 3-AB-68 presents center wavelength ratios of $156.3:55.7:31.5:14:8.7:7 = 22.32:7.95:4.5:2:1.24:1$.

Based on frequency ratio method and the combined interpretation of the MTM and EHA analyses, in addition to the information regarding the average sedimentation rate of 35 cm/kyr (Castro, 2005), we interpreted that the 405-kyr long eccentricity (E) bands are encompassed between 594 and 86 m (for well 1-RJS-297 - Figs. 3), 448 and 94 m (for well 4-RJS-330A - Figs. 4) and 583 and 93 m (for well 3-AB-68 - Fig. 5). The short eccentricity signals (e125 and e95) present bands of 62 to 42 m and 40 to 31 m (well 1-RJS-297 - Figs. 3), 66 to 47 m and 47 to 22 m (well 4-RJS-330A - Figs. 4), 72 to 42 m and 40 to 29 m (well 3-AB-68 - Fig. 5). The obliquity bands are, respectively, 19 to 13 m (for well 1-RJS-297 - Figs. 3), 17 to 13m (for well 4-RJS-330A - Figs. 4) and 18 to 13m (for well 3-AB-68 - Fig. 4). Finally, we interpret the precession parameters (P1 and P2) as bands of 10 to 6.6m (well 1-RJS-297 - Figs. 3), 9.4 to 7m (well 4-RJS-330A - Figs. 4),

and 9.6 to 6.6m (well 3-AB-68 - Fig. 5). The accuracy of these interpretations was confirmed by the optimal sedimentation rates (around 40 cm/kyr) calculated by SAR analyses (Fig. 6).

In the three spectral analyses we also observed the presence of periodicities of approximately 60 and 70 kyr, which are related to bands from 32 to 21m (well 1-RJS-297 - Fig. 3), 31 to 22 (well 4-RJS-330A - Fig. 4) and from 29 to 20 m (well 3-AB-68 - Fig. 4). Such harmonic content can be associated with eccentricity-precession modulations (Hennebert, 2012; Hinnov, 2000; Leandro et al., 2022).

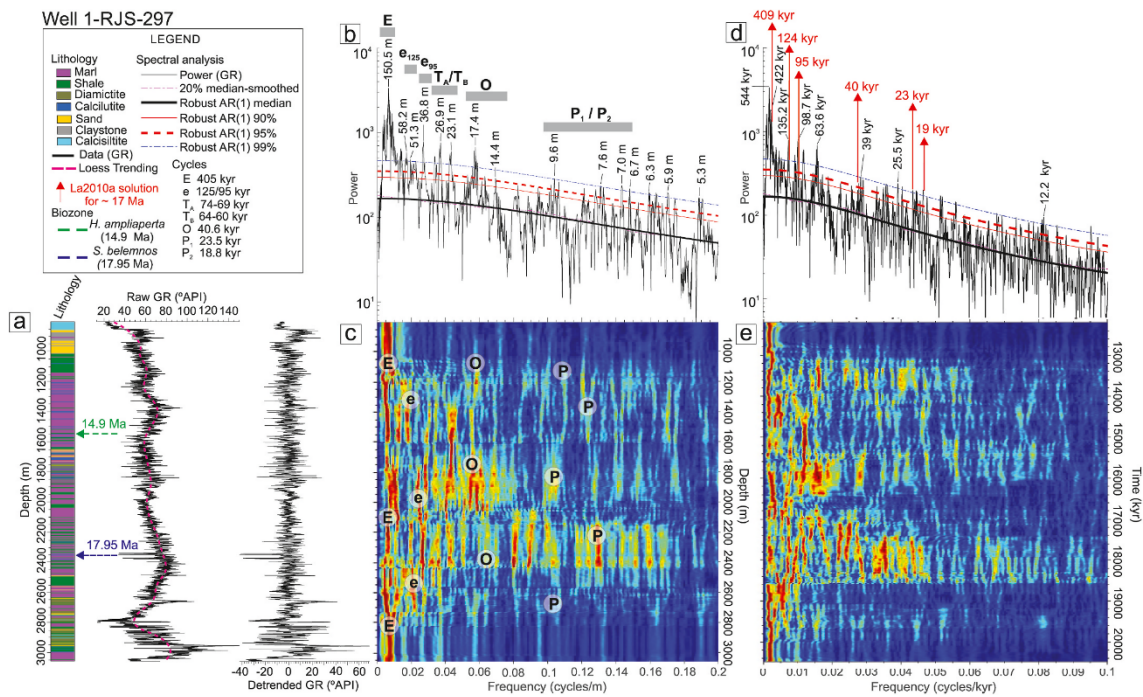


Figure 3 - Spectral analysis of well 1-RJS-297; lithology, raw dataset and detrended dataset by using the LOESS method and a 400 m window (a), 2π multitaper power spectrum with robust AR (1) red noise spectral model (b), evolutionary fast Fourier transform (eFFT) spectrograms with 250 m sliding window (c), 2π multitaper power spectrum of 405-kyr tuned GR dataset (d), and evolutionary fast Fourier transform (eFFT) spectrograms of 405-kyr tuned GR dataset (e).

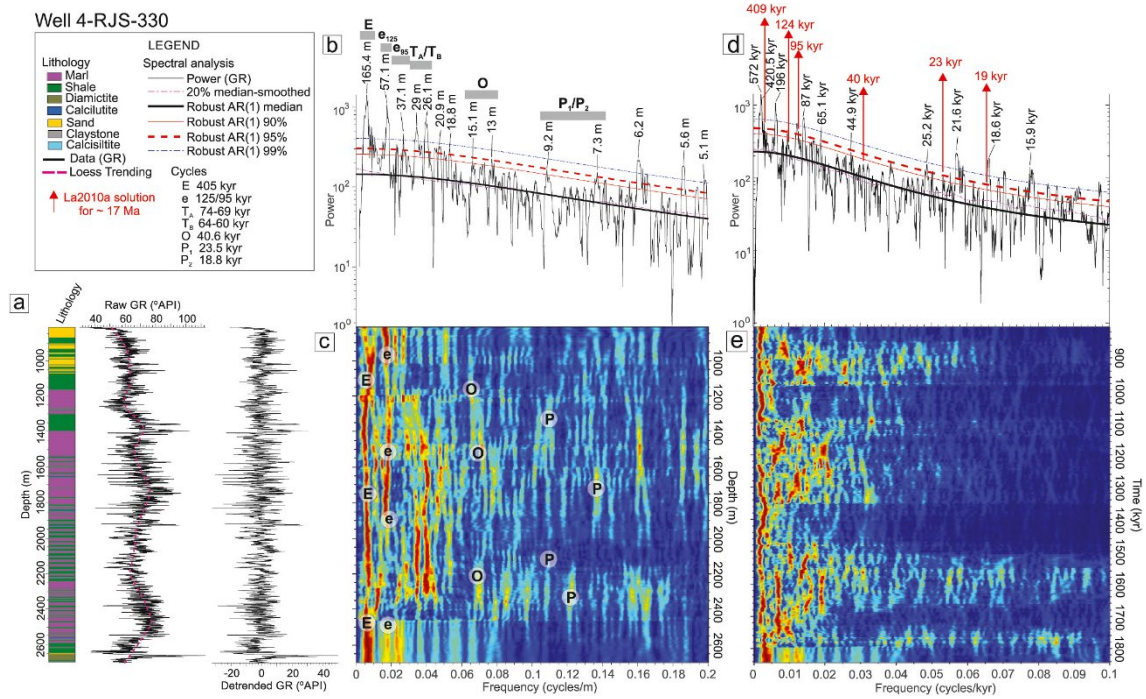


Figure 4 - Spectral analysis of well 3-RJS-330A; lithology, raw dataset and detrended dataset by using the LOESS method and a 400 m window (a), 2π multitaper power spectrum with robust AR (1) red noise spectral model (b), evolutionary fast Fourier transform (eFFT) spectrograms with 250 m sliding window (c), 2π multitaper power spectrum of 405-kyr tuned GR dataset (d), and evolutionary fast Fourier transform (eFFT) spectrograms of 405-kyr tuned GR dataset (e).

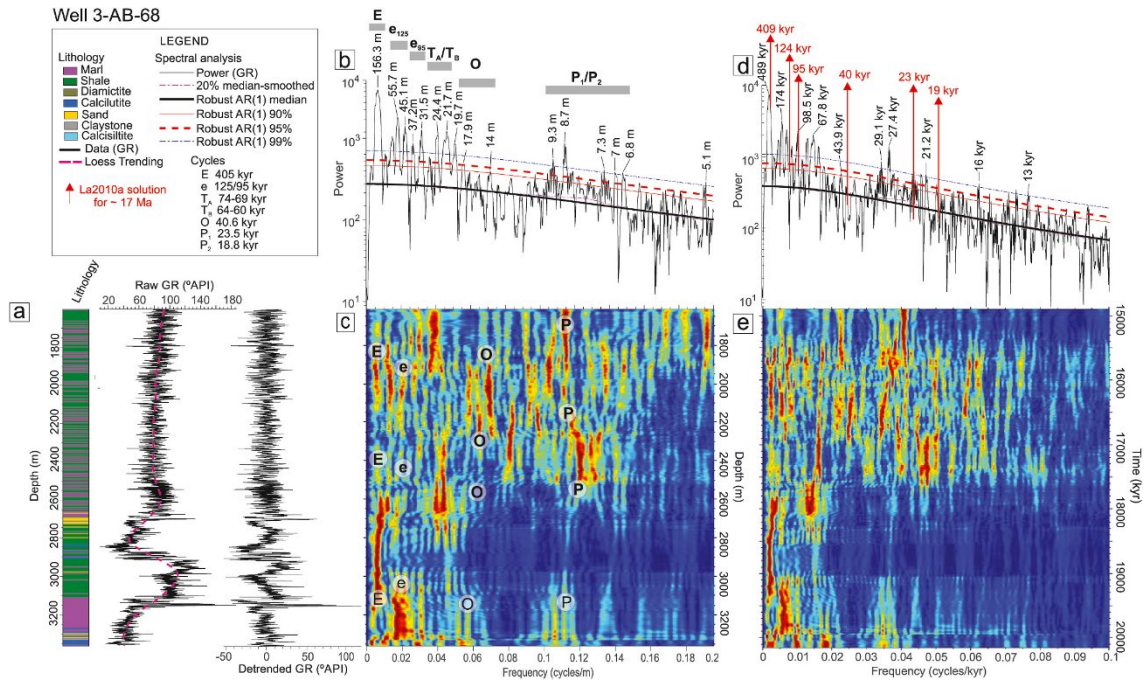


Figure 5 - Spectral analysis of well 3-AB-68; lithology, raw dataset and detrended dataset by using the LOESS method and a 400 m window (a), 2π multitaper power spectrum with robust AR(1) red noise spectral model (b), evolutionary fast Fourier transform (eFFT) spectrograms with 250 m sliding window (c), 2π multitaper power spectrum of 405-kyr tuned GR dataset (d), and evolutionary fast Fourier transform (eFFT) spectrograms of 405-kyr tuned GR dataset (e).

4.22 Sediment accumulation rates analysis

The evaluations of sediment accumulation rates (SAR) were performed using the COCO and eCOCO, taking into account the high values of correlation coefficient (ρ) and low values of H_0 significance level. The results generated sedimentation values that have an actuation of 7 orbital cycles (405, 125, 95, 40.4, 23.5, 22.2 and 19 kyr) in the deposition of the three wells which were under study. Hence, the modulation of these deposits by Milankovitch cycles is confirmed.

For well 1-RJS-297, we observed two significant sedimentation peaks (28 cm/kyr and 37.0 cm/kyr) (Fig. 6a). For this well, the results obtained by the linear sedimentation age model generated minimum and maximum values of 20 cm/kry and 55 cm/kyr (Figs. 6a and 7b). In well 4-RJS-330A, the COCO analysis produced the highest significance level

at 14.0 and 41.9 cm/kyr, while the linear sedimentation rate generated minimum and maximum values of 22 and 50 cm/kyr (Figs. 6b and 8b). The COCO analysis showed two significant peaks for the offshore well 3-AB-68 with a central value of 13.9, 33.1 and 45.4 cm/kyr. In the age model for well 3-AB-68, the minimum and maximum linear sedimentation rate ranged between 16 and 46 cm/kyr (Fig. 9b). The eCOCO results also indicate a significant variation in sediment accumulation rates from a depth of approximately 2500 m for wells 1-RJS-297 and 4-RJS-330A and 2700 m for well 3-AB-68 (Fig. 6). The presence of distinct sedimentation rates found in the SAR analyses of wells 4-RJS-330A (Fig. 6c and 6d) and 3-AB-68 (Fig. 6e and 6f) likely represents a change in the sedimentary dynamics of the environment. However, it is important to highlight that the rates between 34.4 and 43.5 cm/kyr (well 3-AB-68), and 41.9 (well 4-RJS-330A) are the predominant rates. This fact can be observed in both the SAR analyses (Fig. 6) and the wavelength of the long eccentricity signal (165 m - well 4-RJS-330A and 156 m - well 3-AB-68; Figs. 4b and 5b).

Another piece of evidence regarding the dynamics of sedimentary processes in the study area is the presence of discontinuities in the eCOCO results (Fig. 6). These gaps in results can be caused by increased noise resulting by rising environmental instability (Li et al., 2018a; Li et al., 2018b; Liu et al., 2023).

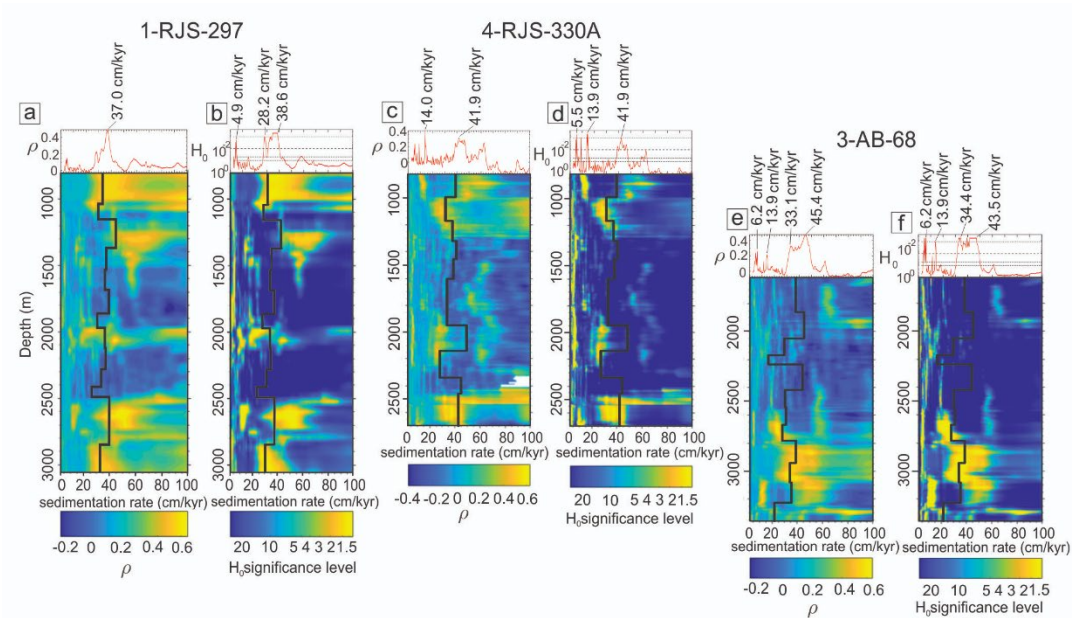


Figure 6 – The COCO and eCOCO results for wells 1-RJS-297, 4-RJS-330A, and 3-AB-68. a) Correlation coefficient (top) and their eCOCO (bottom), and b) Null hypothesis (H_0 , no astronomical forcing; top) and evolutionary H_0 (bottom) for the 1-RJS-297 well. Same for wells 4-RJS-330A (c and d) and 3-AB-68 (e and f). The number of contributing astronomical parameters is seven for three wells. The black line represents the variations in sediment accumulation along the stratigraphy based on the cycle-ratio method.

4.23 Astronomical Tuning

The interpreted frequencies obtained from the spectral analyses and identified as long and short eccentricity cycles were used for band-pass filtering of all presented wells. In well 1-RJS-297, these two filters and the biozones as well as the comparison of the data with the astronomical solution of Laskar 2010a (Laskar et al., 2011) enabled the construction of a 405 kyr tuned age model. We selected the 405 kyr long eccentricity cycle for tuning GR data because the studied region (slope break) has significant dynamics, causing minor erosive events. Therefore, the long eccentricity cycle was the one that best fit our data.

Comparison of the filtered data from well 1-RJS-297 with the astronomical model (Laskar et al., 2011) allowed for the identification of eight long eccentricity cycles and

the amalgamation of cycles E₅ and E₆ (Fig. 7). The interpretation of amalgamation cycles was based on the fact that, at a depth ~1700 m, the long eccentricity cycle has a longer wavelength (~220 m) than the average of the others (~ 124 m). Furthermore, this long eccentricity cycle contains six short eccentricity cycles instead of expected 3 or 4 cycles (Fig. 7d). It is understood that clustering has occurred between cycles E₅ and E₆ due to minor erosional and by-pass processes, which are considered to be common events at continental slope breaks. The presence of small sand layers, with the thickness varying between ~4 and 8 m, between the depths of 1650 and 1750 m, which overlie the fine sediment deposits, constitutes evidence of this minor erosive event (Fig. 7a).

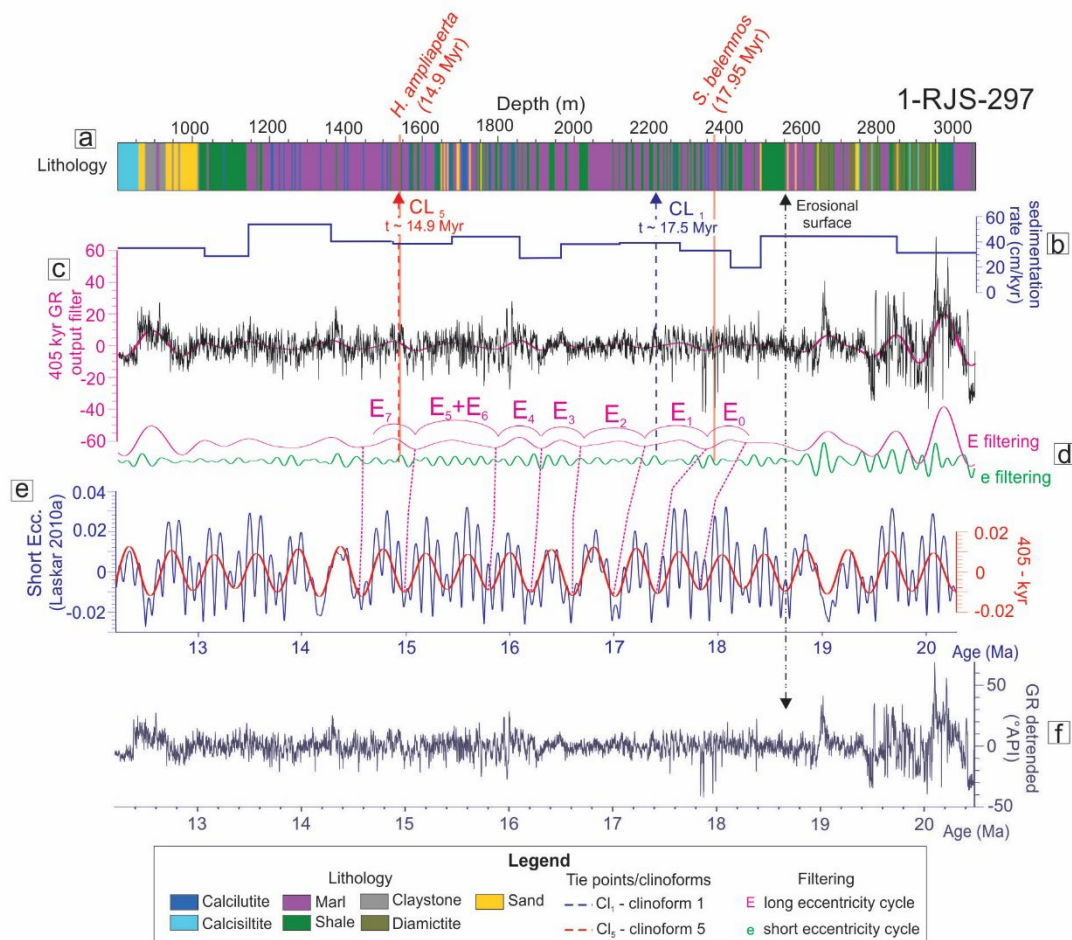


Figure 7. Astronomical calibration of well 1-RJS-297, a) the lithology, b) sedimentation rate derived from conventional cycle-ratio method, c) detrended GR (black) and filtered 150 m wavelengths (red, Gauss filter with a frequency of 0.00664 ± 0.00495 cycles/m) represent 405

kyr long eccentricity cycles, d) filtered 150 m (red, see panel c) and 41 m (green, Gauss filter with a frequency of 0.048019 ± 0.01200 cycles/m) wavelengths representing long and short eccentricity cycles, respectively, e) Laskar 2010a eccentricity model (blue) and filtered 405 kyr cycles (red, Gauss filter with a frequency of 0.01149 ± 0.00849 cycles/kyr), and f) tuned GR log.

The two recorded biozones in well 1-RJS-297 were used to anchor the ATS. Six and a half 405 kyr cycles were identified within the range of these two biozones (Fig. 7d). It is considered that the datum had a good fit with the long eccentricity cycle. As the CL₅ is located at the same depth (1540 m) as the *Helicosphaera ampliaperta* species, an age of 14.9 Ma is established for this clinofom. The *Sphenolithus belemnos* species (associated age of 17.95 Ma) is located near the E₁ cycle pit and a 405 kyr cycle of the CL₁ clinofom (Fig. 7c and d). From this contact, it was possible to establish an age of 17.5 Ma for CL₁ ($17.95 \text{ Ma} - 0.405 \text{ Ma} = 17.5 \text{ Ma}$). The range covered by the CL₁ and CL₅ clinofoms in well 1-RJS-297 comprises part of the E₂ cycle and goes up until E₇.

The band pass filter of long and short eccentricity was used for well 4-RJS-330A. The filter results were also compared with Laskar's 2010a astronomical model for tuning (Fig. 8). The anchors of the ATS were the ages associated with CL₁ and CL₅. Cycles from E₂ to E₇ (Fig. 8d) between these two clinofoms can be noted. The cycles E₅ and E₆ are not well delimited and therefore have been put together in our analysis.

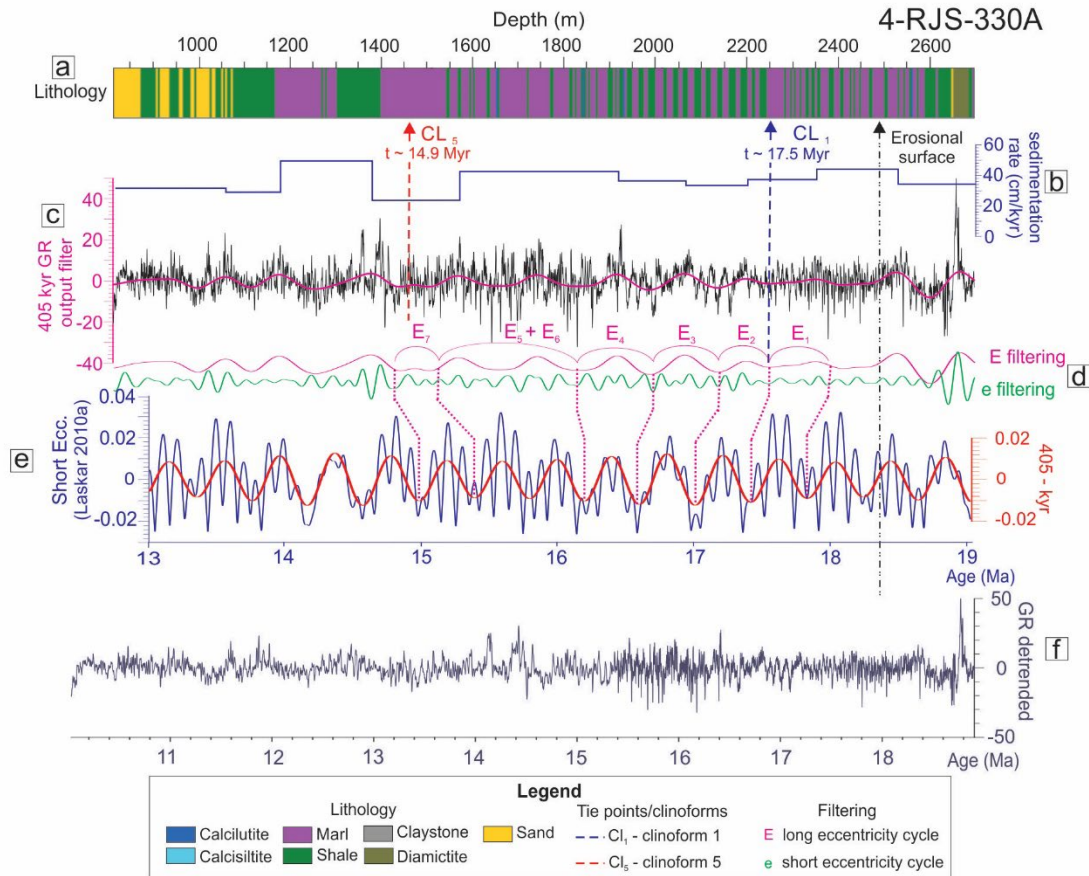


Figure 8 -Astronomical calibration from well 4-RJS-330A , a) the lithology, b) sedimentation rate derived from conventional cycle-ratio method, c) detrended GR (black) and filtered 165 m wavelengths (red, Gauss filter with a frequency of 0.00640 ± 0.00417 cycles/m) represent 405 kyr long eccentricity cycles, d) filtered 165 m (red, see panel c) and 43 m (green, Gauss filter with a frequency of 0.02323 ± 0.00814 cycles/m) wavelengths representing long and short eccentricity cycles, respectively, e) Laskar 2010a eccentricity model (blue) and filtered 405 kyr cycles (red, Gauss filter with a frequency of 0.01149 ± 0.00849 cycles/kyr), and f) tuned GR log.

For Well 3-AB-68, we have also used CL_1 and CL_5 to transpose the ages and anchor the ATS. As like the other two wells, the cycles E_2 to E_7 were identified between the clinoforms CL_1 and CL_5 . Cycles E_4 and E_3 are ‘amalgamated’ and this interpretation was made through the joint evaluation of the long and short eccentricity filter output curves, as was done for well 4-RJS-330A (Fig. 9). In the cyclostratigraphic analysis of

the three wells under study, we chose not to extrapolate the identification of the cycles at depths below the erosive surface, identified in the seismic interpretation, since there are no chronostratigraphic controls or any information about the dimension of this erosive event.

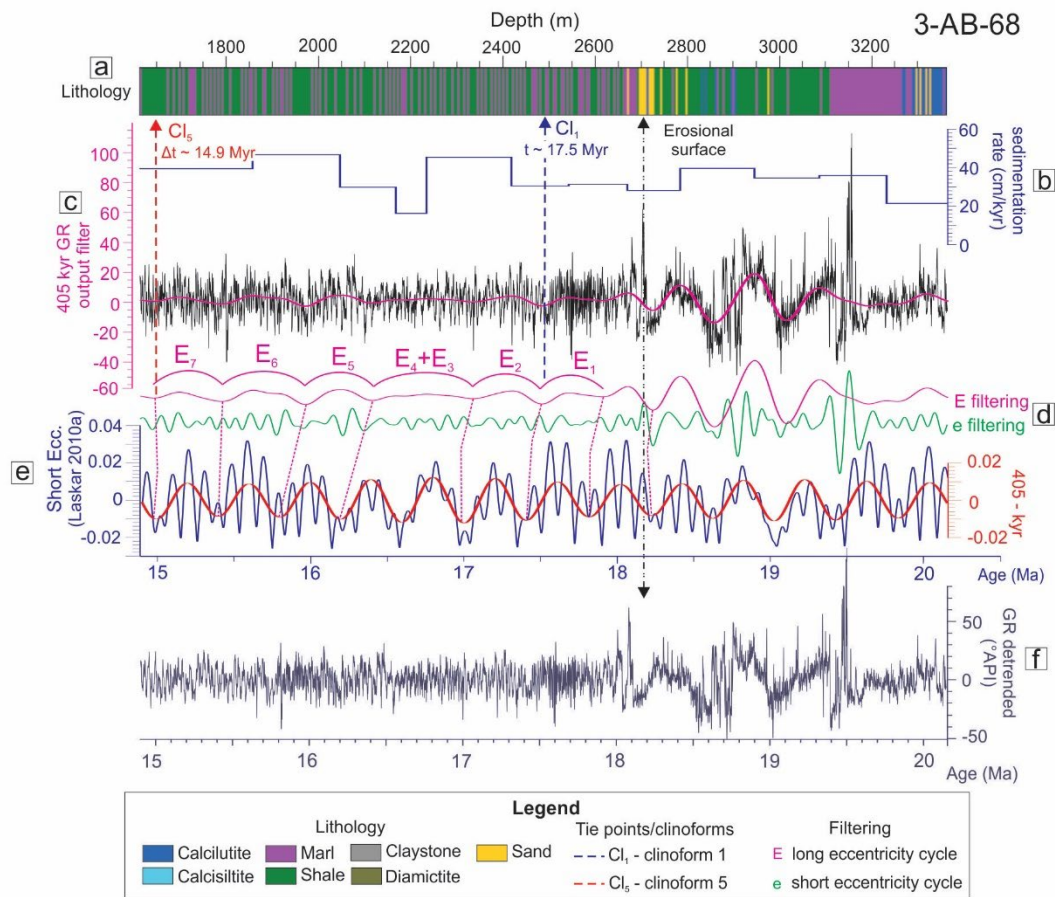


Figure 9 - Astronomical calibration from the 3-AB-68 well, a) the lithology, b) sedimentation rate derived from conventional cycle-ratio method, c) detrended GR (black) and filtered 156 m wavelengths (red, Gauss filter with a frequency of 0.00640 ± 0.00417 cycles/m) represent 405 kyr long eccentricity cycles, d) filtered 156 m (red, see panel c) and 42 m (green, Gauss filter with a frequency of 0.02323 ± 0.00814 cycles/m) wavelengths representing long and short eccentricity cycles, respectively, e) Laskar 2010a eccentricity model (blue) and filtered 405 kyr cycles (red, Gauss filter with a frequency of 0.01149 ± 0.00849 cycles/kyr), and f) tuned GR log.

In order to validate the astronomical tuning, MTM and EHA were performed on the 405-kyr tuned GR series data. These results are presented in Figures 3d, 4d, and 5d, highlighting the strong presence of both long and short eccentricity cycles in the power spectrum across all three wells. Signals of obliquity and precession were also identifiable. Therefore, it is considered that this tuning was appropriate, and similar to the SAR analyses, it supports the presence of orbital cycles in the data series of the three wells studied within this manuscript.

5. DISCUSSION

5.1 2D ATS for the southern Albacora section

Three wells exhibited a clear orbital forcing imprint on the sediment deposition, establishing the feasibility of the correlation between the wells based on the identification of the 405-kyr long eccentricity cycles and its correspondence with seismic reflectors. Therefore, cyclostratigraphic along with seismostratigraphic analyses, in wells arranged in a dip section, enabled the generation of a 2D ATS for the Miocene section in the southern portion of the Albacora Field (Fig. 10). The good correlation of the cyclostratigraphic data can be observed by the sequence of six bundlings interpreted as long eccentricity cycles (E_2 to E_7) between clinoforms CL_1 and CL_5 .

Such data integration was fundamental for the generation of the 2D ATS in light of the application of the seismic interpretation as an age-anchor for wells 4-RJS-330A and 3-AB-68, with good accuracy. The seismic resolution processing was also significant for the construction of the ATS. Figure 11 displays this integration between seismic interpretation and cyclostratigraphic analyses. Our seismic resolution study indicated that the clinoforms can be displaced 15 m above or below the estimated position and hence we did not consider cycles within or below this range for tuning processing. Considering

that short and long eccentricity imprints respectively present wavelengths of ~ 50 m and ~ 150 m, both lie outside the error margin given by the seismic resolution estimate.

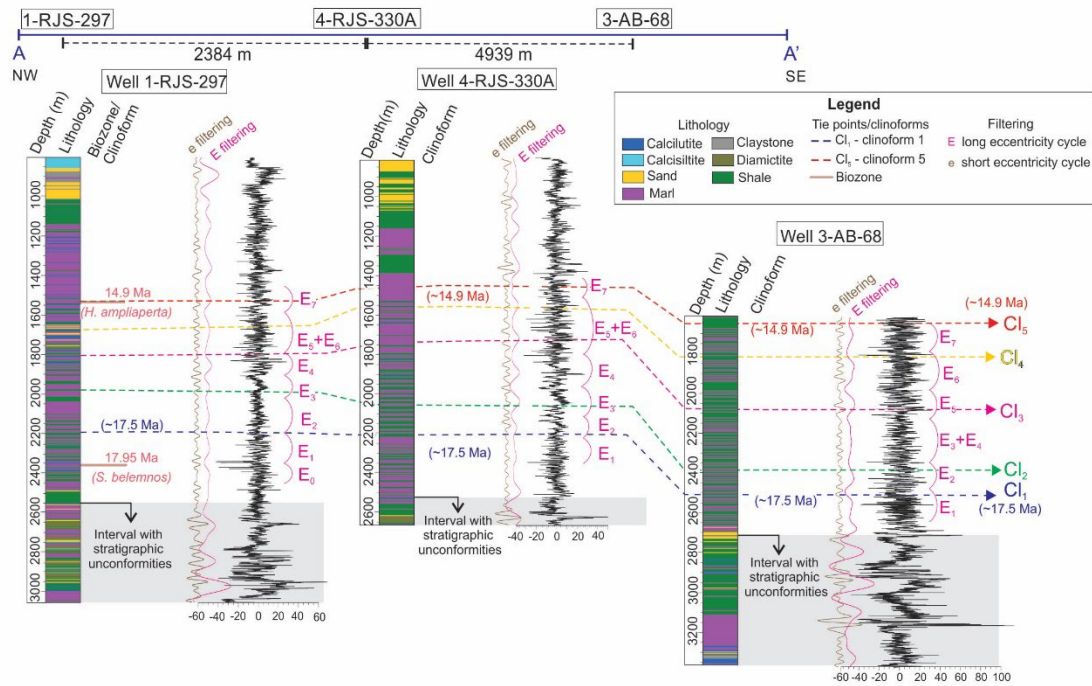


Figure 10. 2D astronomical time scale for the three wells studied in this research with the clinoforms (dashed color lines). A-A' represents the location of the wells within the seismic section (see Fig. 1). The elements contained in each of the wells (from left to right) are: lithology, biozones/clinoforms, short and long eccentricity filters (lines brown and pink, respectively), GR detrended (black line), and delimited long eccentricity cycles ($E_{0,1,2,3\dots}$).

More importantly, it is worth observing that only a few papers integrate seismic and cyclostratigraphic studies (e.g., Ulfers et al., 2002; Bahk et al., 2015; Xia et al., 2020, Du et al., 2020). Moreover, there are no studies that used the application of seismic interpretation to establish ages in the cyclostratigraphy, nor are there seismic resolution studies to identify which tuning is appropriate for the dataset. Hence, our research uses a new and promising methodology for establishing ages and margins of error. Furthermore, the interpretation of the seismic reflectors made it possible to

investigate how the evolution of this slope break occurred over geological time. However, we must be aware that the use of this methodology can also generate errors that are linked to the interpretation of biozone data and of the seismic reflectors.

The sedimentation accumulation rate was assessed through COCO analyses. The results revealed sedimentation rate peak values ranging from 28 to 45 cm/kyr across the three wells. These findings support the values (~30 cm/kyr) reported in other studies conducted in the same region (Castro, 2005; Almeida and Kowsmann, 2014). The choice of the selected wells in a dip profile allowed us to evaluate changes in sediment accumulation rates along this arrangement. The results obtained from the COCO do not show significant differences between wells. Still, the range of values obtained by the age model for each well (Figs. 6 and 7b, 8b, 9b) indicates a small decrease in sediment accumulation towards the more offshore portion (3-AB-68) of the basin.

The evolutionary coefficient correlation (eCOCO) results allowed the identification of more significant sedimentation noise at depths greater than ~2500 m for wells 1-RJS-297 and 4-RJS-330A, and ~ 2700m for well 3-AB-68 (Fig. 6). Increased noise in the dataset indicates erosion and/or depositional gaps (Li et al., 2018a). The erosional surface is located nearby the same depths (Fig. 2). Therefore, this result confirms our interpretation that this seismic horizon represents an erosive event.

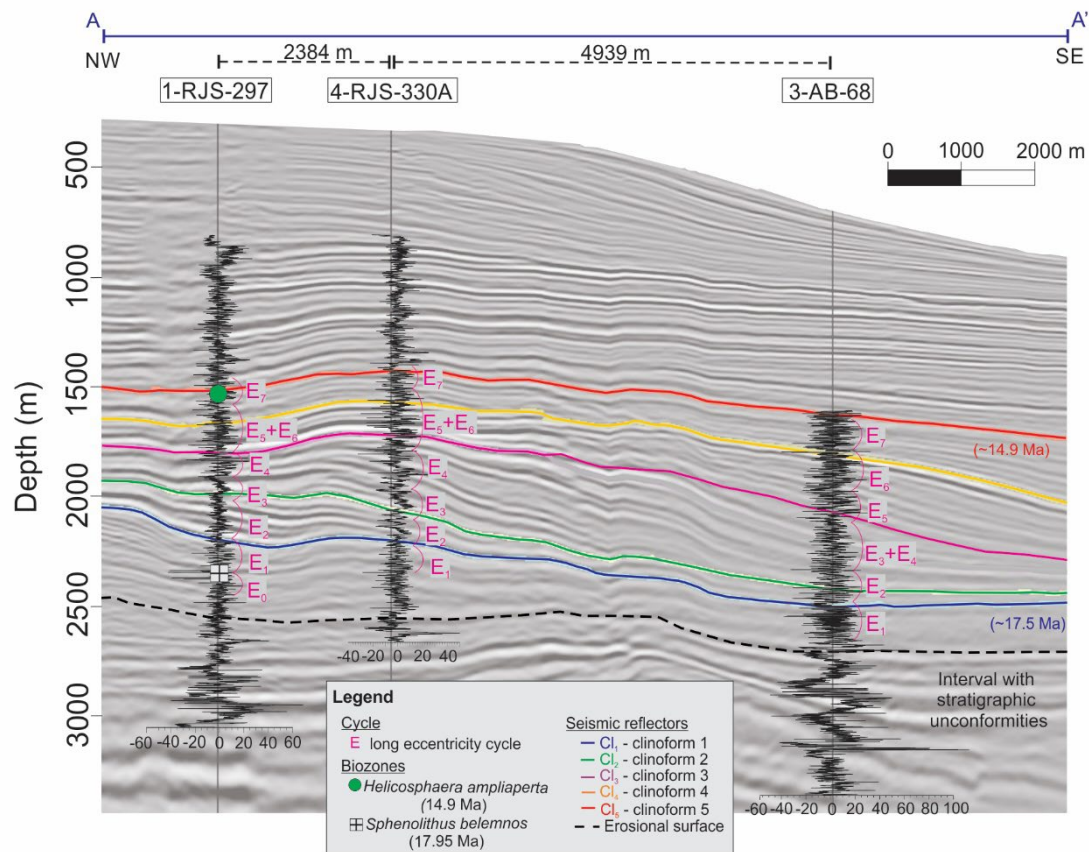


Figure 11 – Correlation between the interpretation of the seismic section and the ATS for the three wells studied in this research. Continuous color lines represent the clinoforms, black dashed lines are the erosional surface, continuous black lines are the GR detrend, and E_{0,1,2,3...} are the delimited long eccentricity cycles.

5.2 Astronomical forcing, deposition, and sea-level changes

The generation of an astronomical calibration for the analyzed wells made it possible to contextualize chronologically the sedimentary evolution in a Miocene section of the slope break of the southern portion of the Albacora Field. The interval with stratigraphic conformities presents in the most basal portion (depths of ~ 2500 to 2700 m) is equivalent to ages around 18.5 Ma and is associated with sand deposits (with layers thinner than 10 m) in all three wells (Figs. 10, 11), as well as an increased noise in the eCOCO result (Fig. 6). This is the limiting depth for tuning because we do not know how much information was lost.

In wells 1-RJS-297 and 4-RJS-330A, sandstone deposits are presented as thicker packages (around 20 m) at depths of about 1000 m associated with ages between 13 and 14 Ma. The interval between these thicker sand deposits is basically composed of interlayered marls and shales.

Comparing the ages obtained in this research with the Cenozoic eustatic curve (Miller et al., 2020), it was possible to observe a correspondence between this interval with the intercalation of marls and shales between depths of ~1000 and ~2500 to 2700 m and the Miocene Climatic Optimum (MCO). The MCO occurred between 17 and 13.8 Ma and represented an interruption in the cooling process of the planet (Miller et al., 2020). This event resulted from the increase in atmospheric CO₂ caused by phases of volcanism along the northwestern American margin (Hodell and Woodruff, 1994; Holbourn et al., 2007; Holbourn et al., 2015). The increase in CO₂ generated a significant reduction in the planet's ice, which resulted in rising sea-levels (Holbourn et al., 2015; Miller et al., 2020). This high sea-level context propitiated the deposition by settling processes of fine sediments (marls and shales) in the slope break of the southern portion of the Albacora Field.

The package that corresponds to the MCO deposits is bounded at the top and bottom by deposits that characterize the energy enhancement of the system. The lower boundary lies at approximately ~ 2500 and 2700 m depth and is characterized by an erosional surface associated with sand packs, whereas the upper limit is at ~1000 m depth and can be identified by the occurrence of thicker sand packs (Fig. 10). The Cenozoic eustatic curve has two significant drops in sea-level that corroborate this increase in system energy recorded at these two boundaries (Miller et al., 2020). In the lower Miocene, the most significant sea-level drop before the MCO occurred in 19 Ma and was over ~60 m below mean sea level. The sedimentary records below the depth of ~ 2500 to 2700 m, related to

ages greater than 18 Ma (Fig 10), were conditioned to a low sea level context. This fact made this sedimentary environment more energetic and consequently under a more significant influence of erosional events. This was recorded in our data through the seismic interpretation (erosional surface), the SAR analyses (increased noise), the lithology (increased sediment grain size), and the variation in the behavior of the RG data (increased amplitude). Hence, possibly during the low sea level period, more than one erosional event occurred in the system. Therefore, we named this depositional interval "interval with stratigraphic unconformities" (Figs. 10 and 11) and discarded it from the ATS construction.

The interval with stratigraphic unconformities (Figs. 10 and 11) evidences a significant environmental change caused, probably, by the formation of gravity flow. Gravity flow deposits intensifies during the low sea-level and is responsible for constructing chaotic facies and sediments with larger grain sizes (sands). Hence, eustatic falls cause more noise in the data series thus generating significant variation (Li et al., 2018a).

The sand packages of the upper boundary corroborate with ages related to the termination of the MCO, dated at 13.8 Ma, characterized by increased benthic foraminifera $\delta^{18}\text{O}$ and a ~ 50 m eustatic fall (Miller et al., 2020). Therefore, the lower and upper boundaries are associated with increased system energy and may have been generated by mass flow transports. The eustatic falls of the late Miocene intensified the formation of turbidite and contourite deposits in the Campos Basin (De Castro and Picolini., 2015; Pandolpho et al., 2021). Considering our study goals and the lack of elements to characterize these sands as turbidites and contourites, we can only state that these sands represent energy changes in the environment associated with two significant eustatic falls that occurred in the Miocene.

6. CONCLUSION

Based on the cyclostratigraphic analyses of three wells and seismic interpretation, a 2D ATS was generated for the Miocene deposits of the southern portion of the Albacora Field. We have identified Milankovitch cycles in all three wells from the time series analyses of variations in GR profiles. Tuning was performed by using the recognized long eccentricity cycle, and the ATS was anchored by utilizing biostratigraphy and seismic interpretation. Sedimentation rates range from 28 cm/kyr to 45 cm/kyr.

The seismic interpretation together with the cyclostratigraphy enabled a correlation between the wells and the association of ages for wells that did not contain biostratigraphic data. Therefore, it was possible to correlate data obtained in other wells and generate an age-depth model for a larger sedimentary basin area.

Our 2D ATS allowed us to have a better understanding of the sedimentary and paleoclimatic evolution of the Miocene deposits of the Albacora Field, as well as provided new information about the Miocene Climatic Optimum in the context of the Campos Basin. This event affected the weathering, transport, and deposition of sediments worldwide. Furthermore, the development of a high-resolution chronostratigraphy for deposits in oil and gas exploration fields provides subsidies for generating more accurate chronostratigraphic frameworks and geological models.

Noteworthy the use of seismic interpretation together with cyclostratigraphy in our study provided a good correlation between the wells and the association of tie-points for wells without biostratigraphic data, allowing the generation of an age-depth model for a large interval of the sedimentary basin area. The application of seismic resolution procedures seemed to be an efficient auxiliary tool for establishing correspondences between ATSs from distinctive wells and to perform tuning from seismic reflectors. Our findings support those joint investigations comprising seismic stratigraphy and

astronomical tuning of well-log data has a great potential for providing 2D astronomical time scales, with significant impact on the establishment of better chronostratigraphic frameworks for exploration basins.

Acknowledgements

The authors would like to thank Petrobras S.A for given technical support and infrastructure in this work and, the Brazilian National Agency for Petroleum, Natural Gas and Biofuels (ANP) for providing the data, and the Observatório Nacional-MCTI where this research was developed. We also thank the financed support from CNPq (314462/2020-1 and 313253/2017-0 to D. R. F., 300919/2023-9 and 300919/2023-9 to N.B.S., 143939/2022-0 to R.M.R.), CAPES (88882.383637/2019- 01 to G.F.) and the Foundation Carlos Chagas Filho Research Support of the State of Rio de Janeiro (FAPERJ)—grant E-26/200.931/2022, and E-26/203.302/2017 to D.R.F., 204.404/2021 to M. C., and 260.022/2022 to T.P.S.).

Chapter 8

Final Considerations

The approach of this study involves generating a 2D Astronomical Time Scale through the correlation of three wells using seismic interpretation and cyclostratigraphic analyses. The Multiple Taper Method was used to confirm the presence of orbital cycles, including long and short eccentricity (Ta and Tb), obliquity, and precession. The gamma ray log was tuned using long eccentricity cycles, and the short eccentricity filter was employed to validate the interpretations of the tuned dataset.

The 2D ATS revealed that the studied deposits represent the Miocene Climate Optimum period and the associated sea-level fluctuations. During the MCO, low-energy environments characterized by marl and shale deposits were observed. The presence of sand deposits indicates an increase in energy, likely attributed to the falling sea-level. This event had a global impact on weathering, sediment transport, and deposition processes. The development of a high-resolution chronostratigraphy for deposits in oil and gas exploration fields contributes to the creation of more precise chronostratigraphic frameworks and geological models.

Analysis of sediment accumulation rates indicated values ranging from 28 cm/kyr to 45 cm/kyr, consistent with previous studies in the Albacora Field area. The distinct behavior of sediment accumulation rates in well 1-RJS-297, prior to the slope break, compared to the other two wells, suggests different sediment dynamics. However, this does not undermine the correlation and the content of Milankovitch Cycles.

The present study demonstrates the integration of seismic interpretation and cyclostratigraphic analyses as an effective approach for understanding sedimentary cycles. It generated a high-resolution chronostratigraphy for the Miocene deposits in the central portion of the Campos Basin. This approach enabled good correlation between wells and the establishment of age-depth models for a significant portion of the sedimentary basin, even in wells lacking biostratigraphic data. The application of seismic resolution procedures proved useful in establishing correlations between ATSs from different wells and in refining seismic reflector tuning.

Bibliography

- ABRAHAM, R., MARSDEN, J. E., RATIU, T., 1988, "Manifolds, Tensor Analysis, and Applications", ed. 2 New York, Springer-Verlag.
- ALMEIDA, A.G., KOWSMANN, R.O., 2014, "Geomorfologia do talude continental e do Platô de São Paulo", In: Kowsmann, R.O., editor. Geologia e Geomorfologia. Rio de Janeiro: Elsevier. Habitats, v. 1. p. 33-66.
- ALVES, T.D., COOPER, M.K.E., RIOS-NETTO, A.D.M., 2016., "Paleogene-Neogene calcareous nanofossil biostratigraphy and paleoecological inferences from northern Campos Basin, Brazil (well Campos-01)", Journal of South American Earth Sciences, 71, pp. 143-160.. doi: 10.1016/j.jsames.2016.06.010
- AMARAL, P.J., MAUL, A., FALCÃO, L., GONZÁLEZ, M., GONZÁLEZ, G., 2015, "Estudo estatístico da velocidade dos sais na camada evaporítica na Bacia de Santos", In: 14th International Congress of the Brazilian Geophysical Society 2015. Rio de Janeiro,
- ASMUS, H.E., 1975, "Controle estrutural da deposição mesozoica nas bacias da margem continental brasileira", Revista Brasileira de Geociências, v.5, n.3, pp. 160-175.
- BAHK, J.J.; UM, I.K.; YI, B.Y.; YOO, D.G., 2015, Paleooceanographic implications and cyclostratigraphy of variations in well-log data from the western slope of the Ulleung Basin, East Sea, Quaternary International.
- BATISTON, D. A., ANTUNES, R. L., DIAS-BRITO, D., 2016, "Nanofósseis calcários e a bioestratigrafia do oligoceno – plioceno da margem continental brasileira", São Paulo, UNESP, Geociências, v. 35, n. 3, pp. 359-371.
- BAUMGARTEN, H., WONIK, T., 2015, Cyclostratigraphic studies of sediments from Lake Van (Turkey) based on their uranium contents obtained from downhole logging and paleoclimatic implications. International Journal Earth Science, 104:1639-1654. Doi: 10.1007/s00531-014-1082-x
- BEHDAD, A., 2019, A step toward the practical stratigraphic automatic correlation of well logs using continuous wavelet transform and dynamic time warping technique. Journal of Applied Geophysics, v. 167, pp. 26-32, <https://doi.org/10.1016/j.jappgeo.2019.05.007>
- BERGER, A., LOUTRE, M.F., LASKAR, J., 1992, "Stability of the astronomical frequencies over the Earth's history for paleoclimatic studies", Science, v. 255, pp. 560-566.

- BERGER, A.; LOUTRE, M., 1994, "Astronomical forcing through geological time, Orbital forcing and cyclic sequences", (IAS Special Publication), PL de Boer and DG Smith, eds. 19, pp. 15-24.
- BIGG, G.R., 1996, "The Oceans and Climate". Cambridge University Press, Cambridge, pp. 1-266.
- BRANDT, D., ERNESTO, M., CONSTABLE, C., FRANCO, D. R., WEINSCHÜTZ, L. C., RODRIGUES, P. O. C., HINNOV, L. A., JAQUETO, P., STRAUSS, B. E., FEINBERG, J., FRANCO, P. V. P., ZHAO, X., 2019, "New Late Pennsylvanian Paleomagnetic Results From Paraná Basin (Southern Brazil): Is the Recent Giant Gaussian Process Model Valid for the Kiaman Superchron?", *Journal of Geophysical Research: Solid Earth*, v; 124, pp. 6223-6242.
- BRUHN, C.H.L., PINTO, A.C.C., JOHANN, P.R.S., BRANCO, C.C.M., SALOMÃO, M.C., FREIRE, E.B. 2017, "Campos and Santos basins: 40 Years of reservoir characterization and management of shallow- to ultra-deep water, post- and pre-salt reservoirs - Historical overview and future challenges", *OTC Brasil 2017*, pp. 327-350. <https://www.onepetro.org/conferences/OTC/17OTCB>. ISBN: 978-151085255-6. doi: 10.4043/28159-ms.
- CATUNEANU, O., 2016, "Principles of Sequence Stratigraphy", Alberta, Elsevier Science.
- CANDY, J. V., 1988, "Signal Processing: The Modern Approach", New York, McGraw-Hill.
- CANDY, J. V., 2019, "MULTITAPER SPECTRAL ESTIMATION: An Alternative to the Welch Periodogram Approach". Lawrence Livermore National Laboratory.
- CASTRO, A. H. A., 2005, "Estudo de ciclicidade orbital com base em dados sísmicos exemplo para o mioceno da bacia de campos", *Revista Brasileira de Geociências*, v. 35.
- CASTRO, R.D., PICOLINI, J.P. 2015, 'Main features of the Campos Basin regional geology' In: Kowsmann, R.O., editor. *Geology and Geomorphology*. Rio de Janeiro: Elsevier. *Habitats*, 1, 1-12.
- CLIMACO, C., Andrade, A. 2009, "Identificação De Litologias Em Perfis Através Da Média-C Fuzzy", Conference: 11th International Congress of the Brazilian Geophysical Society. <https://doi.org/10.3997/2214-4609-pdb.195.2051>.
- COHEN, K. M.; FINNEY, S. C.; GIBBARD, P.L.; FAN, J. X., 2013, "The ICS international chronostratigraphic chart Episodes", v. 36, n.3, p. 199-204.

- COGNÉ, N., GALLAGHER, K., COBBOLD, P.R., 2011, “Post-rift reactivation of the onshore margin of Southeast Brazil: evidence from apatite (U–Th)/he and fission-track data”, *Earth Planet. Sci. Lett.* v. 309, pp. 118–130. Doi: 10.1016/j.epsl.2011.06.025.
- COGNÉ, N., GALLAGHER, K., COBBOLD, P.R., RICCOMINI, C., GAUTHERON, C., 2012, “Post-breakup tectonics in Southeast Brazil from thermochronological data and combined inverseforward thermal history modeling”. *J. Geophysics. Res. Solid Earth*, v. 117 n/a-n/a. 10.1029/2012JB009340.
- CONTRERAS, J., ZÜHLKE, R., BOWMAN, S., BECHSTÄDT, T., 2010, “Seismic stratigraphy and subsidence analysis of the southern Brazilian margin (Campos, Santos and Pelotas basins)”. *Marine and Petroleum Geology* 27, 1952-1980.
- DE CASTRO, R.D., PICOLINI, J.P., 2015, “Principais Aspectos Da Geologia Regional Da Bacia De Campos”, In: Kowsmann, R.O. (Ed.), *Geologia e Geomorfologia*. Elsevier, Rio de Janeiro, pp. 1–12 doi.10.1016/B978-85-352-6937-6.50008-2.
- DE GASPERI, A.; CATUNEANU, O., 2014, “Sequence stratigraphy of the Eocene turbidite reservoirs in Albacora field, Campos Basin”, *offshore Brazil AAPG Bulletin*, v. 98, n. 2 (February 2014), pp. 279–313.
- DELABROYE, A., VECOLI, M., 2010, “The end-Ordovician glaciation and the Hirnantian Stage: A global review and questions about Late Ordovician event stratigraphy”. *Earth Science Reviews* 98 (3-4), 269-282.
- DE OLIVEIRA L.C.V., RODRIGUES R., LEMOS V.B.; 2004, “Multivariate analysis of calcareous nanofossils and stable isotopic ($\delta^{18}O$ and $\delta^{13}C$) in the upper Companion -lower Maastrichtian of the Campos Basin, Brazil”, *Boletim de Geociencias da Petrobras*, V, 13, Issue 1, pp. 81 - 104
- DIAS, J.L., SCARTON, J.C., ESTEVES, F.R., CARMINATTI, M., GUARDADO L.R., 1990, Aspectos da evolução tectono-sedimentar e a ocorrência de hidrocarbonetos na Bacia de Campo”. In: Raja Gabaglia, G.P.; Milani, E.J. (eds.). *Origem e evolução de bacias sedimentares*. Rio de Janeiro, Petrobras, p. 333-360.
- DINARÈS-TURELL, J., WESTERHOLD, T., PUJALTE, V., RÖHL, U., KROON, D., 2014, “Astronomical calibration of the Danian stage (Early Paleocene) revisited: Settling chronologies of sedimentary records across the Atlantic and Pacific Oceans”, *Earth and Planetary Science Letters*, v. 405, pp. 119–131.
- DIAS-BRITO, D, 1989, “A micropaleontologia na indústria do petróleo”, *Revista Brasileira de Geociências*, São Paulo, v. 19, n. 2, p. 256-259.

- DU, W., JI, Y., CHEN, G., WU, H., GAO, C., LI, S., ZHANG, Y., 2020, "Cyclostratigraphy and astronomical tuning during the Oligocene in the Jizhong Depression, Bohai Bay Basin, northeastern China" *Paleogeography, Paleoclimatology, Palaeoecology* 554, 109803.
- FALAHATKHAH, O., KORDI, M., FATEMI, V., KOOCHI, H. H., 2021 "Recognition of Milankovitch cycles during the Oligocene–Early Miocene in the Zagros Basin, SW Iran: Implications for paleoclimate and sequence stratigraphy" *Sedimentary Geology* 421, 105957.
- FANG, Z., ZHANG, L., MA, C., 2023, "Development and controlling factors of shale lithofacies cycles in a continental rift basin: A case study of Es4u in the Boxing Subsag of Dongying Sag, Bohai Bay Basin, China" *Frontiers in Earth Science* 11.
- FAROUK, S.; ABDELDAIM, A.; THIBAUT, N.; AREF, M.; ELFIKI, W.; EL-KAHTANY, K., 2022, "Cyclostratigraphy and eccentricity tuning of the middle Miocene succession, Gulf of Suez, Egypt: Astronomical age dating and undetected hiatus", *Marine and Petroleum Geology*, v. 143. <https://doi.org/10.1016/j.marpetgeo.2022.105771>
- FEDOROV, A.V., PHILANDER, S.G., 2000, "Is El Niño changing?" *Science*. v. 288, pp. 1997–2002.
- FRAGOSO, D.G.C., GABAGLIA, G.P.R., MAGALHÃES, A.J.C., SCHERER, C.M.S., 2021, "Cyclicality and hierarchy in sequence stratigraphy: an integrated approach", *Brazilian Journal of Geology*, <https://doi.org/10.1590/2317-4889202120200106>
- FRANCO, D. R., 2007, "Magnetostratigrafia e análise espectral de ritmicos permocarboníferos da bacia do Paraná: Influências dos ciclos orbitais no regime deposicional", Tese de doutorado, Instituto de astronomia, geofísica e ciências atmosféricas, Universidade de São Paulo.
- FRANCO, D. R.; HINNOV, L. A.; ERNESTO, M., 2011, "Spectral analysis and modeling of microcyclostratigraphy in Late Paleozoic glaciogenic rhythmites (Paraná Basin, Brazil)", *Geochemistry, Geophysics, Geosystems*, v.12, n.9, Q09003.
- FRANCO, D.R.; HINNOV, L.A., ERNESTO M, 2012, "Millennial-scale climate cycles in Permian–Carboniferous rhythmites: Permanent feature throughout geologic time", *Geology*, v. 40 n. 1, pp. 19-22.

- FRANCO, D. R.; HINNOV, L. A., 2013, "Anisotropy of magnetic susceptibility and sedimentary cycle data from Permo-Carboniferous rhythmites (Paraná Basin, Brazil): a multiple proxy record of astronomical and millennial scale palaeoclimate change in a glacial setting", Geological Society, London, Special Publications, v. 373, pp. 355-374.
- FONSECA, J., TEIXEIRA, L., MAUL, A., BARROS, P., BOECHAT, J. & GONZÁLEZ, M. 2018, "Modelling Geological Layers into new Velocity Models for Seismic Migration Process: A Brazilian pre-Salt Case (First EAGE/PESGB Workshop on Velocities)", London, United Kingdom. doi: 10.3997/2214-4609.201800010. Geological Society, London, Special Publications, v. 373, pp. 355-374.
- GUARDADO, L.R.; GAMBOA, L.A.P.; LUCCHESI, C.T., 1990, "Petroleum Geology of the Campos Basin, Brazil, a Model for a Producing Atlantic Type Basin", AAPG Memoir Tulsa, American Association of Petroleum Geologists, pp. 3-79.
- GENNARI, R., PERSICO, D., TURCO, E., VILLA, G., IACCARINO, S.M., FLORINDO, F., LURCOCK, P.C., ZERFASS, G. 2018, "High-resolution integrated calcareous plankton biostratigraphy and magnetostratigraphy at the Oligocene–Miocene transition in Southwestern Atlantic Ocean", Geological Journal, v. 53, n. 3, pp. 1079-1101. doi: 10.1002/gj.2945
- GRADSTEIN, F.M.; OGG, J. G.; SCHMITZ, M. D., OGG, G.M., 2018, Geologic Time Scale 2020.
- GONG, Z., 2021, "Cyclostratigraphy of the Cryogenian Fiq Formation, Oman and its implications for the age of the Marinoan glaciation", Global and Planetary Change, v. 204, 103584. <https://doi.org/10.1016/j.gloplacha.2021.103584>
- HENNEBERT, M., 2012, "Hunting for the 405-kyr eccentricity cycle phase at the Cretaceous-Paleogene boundary in the Ain Settara section (Kalaat Senan, central Tunisia)" Carnets de Géologies, 2012/05, 93-116.
- HILGEN, F.J., LOURENS, L.J., VAN DAM, J.A., 2012, "The Neogene period", In: Gradstein, F.M., Ogg, J.G., Schmitz, M., Ogg, G. (Eds.), The Geologic Time Scale 2012, Elsevier, pp. 923-978.
- HILGEN, F. J., SCHWARZACHER, W., STRASSER A., 2004, "Concepts and definitions in cyclostratigraphy (second report of the cyclostratigraphy working group)" – SEPM Spec. Publ. 81, 303–305, Tulsa.
- HINNOV, L. A., 2000, "New perspectives on orbitally forced stratigraphy", Annual Review of Earth and Planetary Sciences, v. 28, n. 1, pp. 419-475.

- HINNOV, L.A.; HILGEN, F. J., 2012, "Cyclostratigraphy and Astrochronology", In: Gradstein, F.M., Ogg, J.G., Smith, A. G. (Eds.), A Geologic Time Scale 2012: Elsevier, pp. 63–83.
- HINNOV, L.A., 2013, "Cyclostratigraphy and its revolutionizing applications in the earth and planetary sciences", GSA Bulletin, v.125 n. 11/12, pp. 1703–1734.
- HINNOV, L. A., WU, H., FANG, Q., 2016, "Reply to the comment on "Geologic evidence for chaotic behavior of the planets and its constraints on the third-order eustatic sequences at the end of the Late Paleozoic Ice Age" by Qiang Fang, Huaichun Wu, Linda A. Hinnov, Xiuchun jing, Xunlian Wang, and Qingchun Jiang [Palaeogeography Palaeoclimatology Palaeoecology 400 (2015)", 848–859], Palaeogeogr. Palaeoclimatol. Palaeoecol., v. 461, pp. 475-480
- HINNOV. L.A., 2018, "Cyclostratigraphy and Astrochronology in 2018", Stratigraphy & Timescales v. 3, pp. 1-80.
- HODELL, DA; WOODRUFF, F., 1994, "Variations in the strontium isotopic ratio of seawater during the Miocene: Stratigraphic and geochemical implications", Paleceanography, v. 9, pp.405– 426. <https://doi.org/10.1029/94PA00292>.
- HOLBOURN, A.; KUHNT, W.; KOCHHANN, K.G.D.; ANDERSEN, N.; MEIER, S., 2015, "Global perturbation of the carbon cycle at the onset of the Miocene Climatic Optimum", Geology, v. 43 ed.2, pp. 123-126. <https://doi.org/10.1130/G36317.1>
- HOLBOURN, A.E., KUHNT, W., SCHULZ, M., FLORES, J.A., AND ANDERSEN, N., 2007. Middle Miocene long-term climate evolution: Eccentricity modulation of the "Monterey carbon-isotope excursion", Earth and Planetary Science Letters, v. 261, pp. 534–550. <https://doi:10.1016/j.epsl.2007.07.026>
- HUANG, C., 2018, "Astronomical Time Scale for the Mesozoic. Stratigraphy & Timescales", v. 3, pp. 81-150, <https://doi.org/10.1016/bs.sats.2018.08.005>.
- HURRELL, J.W., 1995, "Decadal trends in the North Atlantic Oscillation: regional temperatures and precipitation", Science, v.269, pp. 676–679.
- JOSHI, K. B., GOSWAMI, V., BANERJI, U., SHANKAR, R., 2021, "Recent Developments in Instrumentation and its Application in Absolute Dating: Historical Perspective and Overview" Journal of Asian Earth Sciences 211, 104690.
- JOUZEL, J., MASSON-DELMOTTE, V., CATTANI, O., DREYFUS, G., FALOURD S., HOFFMANN, G., MINSTER, B., NOUET J., BARNOLA, J.M., CHAPPELLAZ, J., FISCHER, H., GALLET, J.C.,

- JOHNSEN, S., LEUENBERGER, M., LOULERGUE, L., LUETHI, D., OERTER, H., PARRENIN, F., RAISBECK, G., RAYNAUD, D., SCHILT, A., SCHWANDER, J., SELMO, E., SOUCHEZ, R., SPAHNI, R., STAUFFER, B., STEFFENSEN, J.P., STENNI, B., STOCKER, T.F., TISON, J.L., WERNER, M., WOLFF, E.W. 2007, "Orbital and Millennial Antarctic Climate Variability over the Past 800,000 Years", *Science*, v.317, n. 5839, pp. 793-796. <https://doi.org/10.1126/science.1141038>
- KENT, D. V., OLSEN, P. E., RASMUSSEN, C., LEPRE, C., MUNDIL, R., IRMIS, R. B., GEHRELS, G. E., GIESLER, D., GEISSMAN, J. W., PARKER, W. G., 2018, "Empirical evidence for stability of the 405-kiloyear Jupiter–Venus eccentricity cycle over hundreds of millions of years" *Proceeding of the National Academy of Sciences* 115, 24.
- KOCHHANN, M. V. L.; CAGLIARI, J.; KOCHHANN, K. G. D.; FRANCO, D. R., 2020, "Orbital and millennial-scale cycles paced climate variability during the Late Paleozoic Ice Age in the southwestern Gondwana", *Geochemistry, Geophysics, Geosystems*, v. 21, e2019GC008676.
- KODAMA, K.P., HINNOV, L., 2015, "Rock Magnetic Cyclostratigraphy". Wiley-Blackwell.
- Kotov, S., Pälke, H., 2018, "QAnalySeries – a Cross-Platform Time Series Tuning and Analysis Tool", AGU Fall Meeting, Washington DC.
- KOTOV, S., PÄLIKE, H., 2018, "QAnalySeries – a Cross-Platform Time Series Tuning and Analysis Tool", AGU Fall Meeting, Washington DC.
- LASKAR, J.; JOUTEL, J.; BOUDIN, F., 1993, "Orbital, precessional and insolation quantities for the Earth from -20 Myr to 10 Myr", *Astronomy Astrophys.* V. 270, pp. 522-533.
- LASKAR, J., ROBUTEL, P., JOUTEL, F., GASTINEAU, M., CORREIA, A., LEVRARD, B., 2004, "A long-term numerical solution for the insolation quantities of the Earth". *Astron. Astrophys.* V.428. pp. 261-285.
- LASKAR, J., 2008, "Chaotic diffusion in the Solar System". *Icarus*, v. 196, pp. 1-15.
- LASKAR, J., FIENGA, A., GASTINEAU, M., MANCHE, H., 2011, "La2010: a new orbital solution for the long-term motion of the Earth". *Astron. Astrophys.*, v. 532.
- LEANDRO, C.G., SAVIAN, J.F., KOCHHANN, M.V.L. et al., 2022, "Astronomical tuning of the Aptian stage and its implications for age recalibrations and paleoclimatic events", *Nature Communications* 13, 2941. <https://doi.org/10.1038/s41467-022-30075-3>
- LI, M., KUMP, L.R., HINNOV, L.A., MANN, M.E., 2018, "Tracking variable sedimentation rates and astronomical forcing in Phanerozoic paleoclimate proxy series with

- evolutionary correlation coefficients and hypothesis testing” *Earth Planet. Sci. Lett.* 501, 165-179.
- LI, M., HUANG C., OGG J., ZHANG Y., HINNOV L., U.W.U. H., CHEN Z. O., ZOU Z., 2019a, “Paleoclimate proxies for cyclostratigraphy: Comparative analysis using a Lower Triassic marine section in South China”, *Earth-Science Reviews*, v.189, pp. 125 – 146. ISSN 0012-8252. <https://doi.org/10.1016/j.earscirev.2019.01.011>
- LI, M.; HINNOV, L.; KUMP, L., 2019, “Acycle: Time-series analysis software for paleoclimate research and education”, *Computers and Geosciences*, v. 127, pp. 12-22.
- LINHARES, O. A. G., STOHLER, R. C., CORREA, S. N., IDA, M., COELHO, F. M., 2018, “Otimização da estratégia de drenagem com base no mapeamento sísmico de barreiras hidráulicas relacionadas à elementos arquiteturais em um campo da bacia de campos”. In: *Anais do 49o Congresso Brasileiro de Geologia*.
- LIU, Z.; Huang, C.; ALGEO, T.J.; LIU, J.; HAO, Y.; DU, X.; LU, Y.; CHEN, P.; GUO, L.; PENG, L., 2017, “High-resolution astrochronological record for the paleocene-oligocene (66-23 Ma) from the rapidly subsiding Bohai Bay Basin, northeastern China”, *Palaeogeography, Palaeoclimatology, Palaeoecology* v.510, pp. 78-92.
- LOCKLAIR, R.E.; SAGEMAN, B.B., 2008, “Cyclostratigraphy of the Upper Cretaceous Niobara Formation, Western Interior, U.S.A.: A Coniacian-Santonian orbital timescale”, *Earth Planetary Sciences Letters* v. 269, pp. 540-553.
- LOURENS, L.J.; HILGEN, F.; SHACKLETON, N.J.; LASKAR, J.; WILSON, D.; 2004, “The Neogene Period”, In: Gradstein, F., Ogg, J., Smith, A. (Eds.), *A Geologic Time Scale 2004*, Cambridge University Press, Cambridge, UK, pp. 400-440.
- LUNA, J., BATEZELLI, A., DELGADO, L., REBELO, T. 2019, “Stratigraphic framework and petrophysical analysis of Oligocene-miocene turbidite systems in the eastern Marlim oilfield (SE Brazil)”, *Journal of South American Earth Sciences*, 90, pp. 34-53. doi: 10.1016/j.jsames.2018.11.022
- MAGALHÃES, A. J. C., GABAGLIA, G.P.R., FRAGOSO, D.G.C, FREIRE, E.B., LYKAWKA, R.; ARREGUI, C.D., SILVEIRA, M.M.L, CARPIO, K.M.T., PEDRINHA, S., ARTAGÃO, V.M., TERRA, G.J.S., BUNEVICH, R.B., ROEMERS-OLIVEIRA, E., GOMES, J.P., HERNÁNDEZ, R.M., BRUHN, C.H.L., 2020, “High-resolution sequence stratigraphy applied to reservoir zonation and characterization, and its impact in production performance – shallow marine, fluvial downstream, and lacustrine carbonate setting”, *Earth-Science Reviews* v. 210, 103325.

- MAKLED, W. A., 2021, "Applications of miospore quantitative stratigraphy and cyclostratigraphy in the Neocomian - Cenomanian sediments in the Western Desert, Egypt: A step in the way to biochronostratigraphy", *Marine and Petroleum Geology*, v. 124, 104815.
- MANN, M.E., LEES, J.M., 1996, "Robust estimation of background noise and signal detection in climatic time series" *Climatic Change* 33, 409-445.
- MATTNER, J., AL-HUSSERINI, M., 2002, "Essay: applied cyclo-stratigraphy for the Middle East E&P industry", *GeoArabia*, v. 7, 4.
- MARTINI, E., 1971, "Standard Tertiary and Quaternary calcareous nannoplankton zonation", In: FARINACCI, A. (Editor.), *Proceedings 2nd International Conference Planktonic Microfossils*. Roma: Edizioni Tecnoscienza, pp. 739-785.
- MAUL, A., BULCÃO, A., DIAS, R.M., PEREIRA-DIAS, B., TEIXEIRA, L., BORGES, F., GONZÁLEZ, M., GUIZAN, C., CETALE, M., 2021, "Benefits of inserting salt stratification to detail velocity model prior to least-squares reverse-time migration", *Journal of Applied Geophysics*, V. 195, 104469, ISSN 0926-9851, <https://doi.org/10.1016/j.jappgeo.2021.104469>.
- MAUL, A., CETALE, M., GUIZAN, C., CORBETT, P., UNDERHILL, J. R., TEIXEIRA, L., PONTES, R., GONZÁLEZ, M., 2021, "The impact of heterogeneous salt velocity models on the gross rock volume estimation: an example from the Santos Basin pre-salt, Brazil". *Petroleum Geoscience* 2021, v. 27, n.4, petgeo2020-105. doi: <https://doi.org/10.1144/petgeo2020-105>
- MENEZES, J. R. C., 2004, "Modelagem Estratigráfica de Clincoformas Depositionais: Construção e Aplicação de um Modelo Computacional Baseando em Mecânica Estatística", Tese de Doutorado, Universidade Federal do Rio Grande do Sul.
- MENEZES, S.X., 1985, "Campo de Namorado, Aspectos de Geologia de Reservatórios", Petrobras/DEPEXDIRSUL, Relatório Interno, 9 p.
- MEYERS, S. R., 2012, "Seeing red in cyclic stratigraphy: Spectral noise estimation for astrochronology", *Paleoceanography and Paleoclimatology*, v. 27, n. 3.

- MEYERS, S. R., 2015, "The evaluation of eccentricity-related amplitude modulation and bundling in paleoclimate data: An inverse approach for astrochronologic testing and time scale optimization", *Paleoceanography*, v. 30, n. 12, pp. 1625-1640.
- MEYERS, S. R., 2019, "Cyclostratigraphy and the problem of astrochronologic testing" *Earth-Science Reviews*, 190-223.
- MEYERS, S. R., MALINVERNO, A., 2018, "Proterozoic Milankovitch cycles and the history of the solar system", *Proceedings of the National Academy of Sciences*, v. 115, n. 25, pp. 6363-6368.
- MEYERS, S. R., SAGEMAN, 2007, "Quantification of deep-time orbital forcing by average spectral mist", *American Journal of Science*, v. 307, n. 5, pp. 773-792.
- MILLER, B. V., 2006, "Introduction to Radiometric Dating" *The Paleontological Society Papers*, 12, 1-23. doi:10.1017/S1089332600001327
- MILLER, K. G., BROWNING, J. V., SCHMELZ W. J., KOPP R. E., MOUNTAIN G. S., WRIGHT J. D. 2020, "Cenozoic sea-level and cryospheric evolution from deep-sea geochemical and continental margin records". *SCIENCE ADVANCES*. <https://doi.org/10.1126/sciadv.aaz1346>
- MUTTI, E.; CARMINATTI, M., 2012, "Deep-water sands of the Brazilian offshore basins". In: *AAPG Int. Conf. Exhib. Milan*, p. 30219. 30219.
- OKADA, H.; BUKRY, D., 1980, "Supplementary modification and introduction of code numbers to the low-latitude coccolith biostratigraphic zonation (Bukry, 1973; 1975)". *Marine Micropaleontology*, v. 5, n. 3, p. 321-25.
- OVALLE, A. R. C., SILVA, C.F., REZENDE, C. E., GATTS, C. E. N., SUZUKI, M.S., FIGUEIREDO, R.O., 2013, "Long-term trends in hydrochemistry in the Paraíba do Sul River, southeastern Brazil", *Journal of Hydrology* v. 481, pp. 191-203. <https://doi.org/10.1016/j.jhydrol.2012.12.036>
- OLIVEIRA M.J., CARNEIRO C.D.R., VECCHIA F.A.S., BAPTISTA G.M.M. 2017, "Ciclos climáticos e causas naturais das mudanças do clima", *Terra e Didática*, v. 13, n.3, pp. 149-184. <https://doi.org/10.20396/td.v13i3.8650958>

- OSORIO, J. S.L., 2017, "3D Geological Modeling of the Oligocene-Miocene Turbidite System in the Eastern Marlim Oilfield", Campos Basin, Brazil, Universidade Estadual de Campinas, Campinas, SP, Dissertação de mestrado, 138 p.
- FIGUEIREDO, R.O., 2013, "Long-term trends in hydrochemistry in the Paraíba do Sul River, southeastern Brazil" *Journal of Hydrology* 481, 191-203. <https://doi.org/10.1016/j.jhydrol.2012.12.036>
- PANDOLPHO, B. T.; KLEIN, A. H. F.; DUTRA, I.; MAHIQUES, M. M.; VIANA, A. R.; BUENO, G. V.; MACHADO, A. A.; CAMARGO, Y. L.; HERCOS, C. M.; LIMA, Y.; FILHO, A. F. H. F.; THEODORO, C. E., 2021, "Seismic record of a cyclic turbidite-contourite system in the Northern Campos Basin, SE Brazil", *Marine Geology*, v. 434, <https://doi.org/10.1016/j.margeo.2021.106422>
- PERLMUTTER, M. A., AZAMBUJA FILHO, N. C. 2005. "Cicloestratigrafia: teoria e técnicas", *Revista Brasileira de Geociências*, v. 35.
- PROKOPH, A., AGTERBERG, F. P. 1999, "Detection of sedimentary cyclicity and stratigraphic completeness by wavelet analysis: An application to Late Albian cyclostratigraphy of the Western Canada Sedimentary Basin", *Journal of Sedimentary Research*, v. 69, pp. 862-875. <https://doi.org/10.2110/jsr.69.862>.
- RANGEL, H. D.; MARTINS, F.A.L.; ESTEVES F.R.; FEIJÓ, F.J, 1994, "Boletim Geociências Petrobras, Rio de Janeiro, v. 8 n.2, pp. 203-217.
- RICHTER, A. J.; GOMIDE, J.; SHIMABUKURO, S., ANTUNES, R. L., 1997, "Bioestratigrafia dos nanofósseis cenozoicos da margem continental brasileira", Rio de Janeiro: Petrobras / Cenpes / Divex / Sebipe. In: ANTUNES, R. L. Introdução ao estudo dos nanofósseis, Rio de Janeiro: Instituto de Geociências – Universidade Federal do Rio de Janeiro, 124 p.
- RODRIGUES, P., O., C., 2018, "Testing timescales for 2.5 ga banded iron formations rhythms (dales gorge member, hamersley basin, australia) by using distinct cyclostratigraphic approaches", Tese de Doutorado, Observatório Nacional.
- RUFFEL, A.; WORDEN, R., 2000, "Palaeoclimate analysis using spectral gamma-ray data from the Aptian (Cretaceous) of southern England and southern France", *Palaeogeography, Palaeoclimatology, Palaeoecology* v. 155, pp. 265-283. [https://doi.org/10.1016/S0031-0182\(99\)00119-4](https://doi.org/10.1016/S0031-0182(99)00119-4)
- SILVA, J.G.R., AZAMBUJA FILHO, N.C., 2005, "Cicloestratigrafia do Eopermiano - Estudo de caso no Grupo Itararé, Bacia do Paraná (parte 2): Evidências de indução

- astronômica (orbital e solar) no clima e na sedimentação”, *Rev. Bras. Geoc.*, v. 35, pp. 77-106.
- THOMSON, D.J., 1982, “Spectrum estimation and harmonic analysis”, *Proc. IEEE* 70: 1055–96.
- THOMSON, D.J. 1990, “Quadratic-inverse spectrum estimates; applications to paleoclimatology”, *Philos. Trans. R. Soc. Lond.* 332A: 539–97.
- TORRES L.F., BARROSO E.V. 2021, “Integration of geophysical and geomechanical data to understand the depletion of the Marlim field, Campos Basin”. *Geologia USP - Serie Cientifica Open Access*, V. 21, n. 1, pp. 45 – 55. DOI: 10.11606/issn.2316-9095.v21-166922.
- ULFERS, A.; ZEEEDEN, C.; WAGNER, B.; SKRATTEL, S.; BUNESS, H.; WONIK, T., 2022, “Borehole logging and seismic data from Lake Ohrid (North Macedonia/ Albania) as a basis for age-depth modelling over the last one million years”, *Quaternary Science Reviews*, v. 276: 107295. <https://doi.org/10.1016/j.quascirev.2021.107295>
- VAN ANDEL, T.H.; THIEDE, J., SCLATER, J.G.; HAY, W.W. 1977, “Depositional history of the south atlantic ocean during the last 125 milion years”, *The Journal of Geology*, v. 85, n. 6, pp. 651-698.
- VIANA, A., R., 2001, “Seismic expression of shallow- to deep-water contourites along the south-eastern Brazilian margin”. *Mar. Geophys. Res.*, v. 22, pp. 509–521. <https://doi.org/10.1023/A:1016307918182>.
- WALTHAM, D., 2015, “Milankovitch period uncertainties and their impact on Cyclostratigraphy”, *Journal of Sedimentary Research*, v. 85, n. 8, pp. 990- 998.
- WEEDON, G. P., 2003, “Time-series analysis and cyclostratigraphy: examining stratigraphic records of environmental cycles”, Cambridge University Press. 275 p
- WIDESS, M. B., 1973. How thin is a bed? *Geophysics* 38,6: 1176-1180. <https://doi.org/10.1190/1.1440403>
- WINTER, W. R.; JAHNERT, R.J.; FRANÇA, A. B., 2007, “Bacia de Campos”. *Boletim Geociências Petrobras*, Rio de Janeiro, v. 15, n. 2, pp. 511-529.
- Wu, H.C., Zhang, S.H., Sui, S.W., Huang, Q.H., 2007, “Recognition of Milankovitch cycles in the natural gamma-ray logging of Upper Cretaceous Terrestrial Strata in the Songliao Basin”. *Acta Geologica Sinica* v.81, pp. 996–1001.

- WU, H., ZHANG, S., FENG, Q., JIANG, G., LI, H., YANG, T., 2012, “Milankovitch and subMilankovitch cycles of the early Triassic Daye Formation, South China and their geochronological and paleoclimatic implications”. *Gondwana Res.* V. 22, pp. 748–759. <https://doi.org/10.1016/j.gr.2011.12.003>.
- PRAYROS, A., MARTINEZ-BRACERAS, n., 2014, “Orbital forcing in turbidite accumulation during the Eocene greenhouse interval”, *Sedimentology*, v. 61, pp. 1411-1432.
- PERCIVAL, D.B. and WALDEN, A.T., 1993, “Spectral Analysis for Physical Applications. Multitaper and Conventional Univariate Techniques”, Cambridge University Press, Cambridge, pp. 1–583.
- XIA, S., LIN, C., DU, X., JIA, D., AHMAD, N. ZHANG, Z., GAO, L. ZHU, Y. 2020, “Correspondences among lacustrine fluctuations, climate changes and the Milankovitch cycles in the Paleogene through tracking onlap points and correlating palaeontology in Liaozhong Depression, Bohai Bay Basin, NE China”, *Geological Journal*, v. 55. N. 9, pp. 6527-6543 <https://doi.org/10.1002/gj.3825>
- ZACHOS, J.C., PAGANI, M., SLOAN, L., THOMAS, E., BILLUPS, K., 2001, “Trends, rhythms, and aberrations in global climate 65 Ma to present”. *Science*, v. 292, pp. 686-693, <https://doi.org/10.1126/science.1059412>.
- ZACHOS, J.C., DICKENS, G.R., ZEEBE, R.E., 2008, “An early Cenozoic perspective on greenhouse warming and carbon-cycle dynamics”, *Nature* 451, pp. 279-283.
- Weedon, G., 2003. *Time series analysis and Cyclostratigraphy. Examining Stratigraphic Records of Environmental Cycles*. Cambridge University Press ISBN: 0521620015
- WINTER, W.R.; JAHNERT, R.J.; FRANÇA, A.B., 2007, “Bacia de Campos” *Boletim Geociências Petrobras*, Rio de Janeiro 15 (2), 511-529.
- WU, H.C., ZHANG, S.H., SUI, S.W., HUANG, Q.H., 2007, “Recognition of Milankovitch cycles in the natural gamma-ray logging of Upper Cretaceous Terrestrial Strata in the Songliao Basin” *Acta Geologica Sinica* 81, 996–1001.
- WIDESS, M.B., 1973, “How thin is a bed?” *Geophysics* 38,6: 1176-1180. <https://doi.org/10.1190/1.1440403>

WU, H., ZHANG, S., FENG, Q., JIANG, G., LI, H., YANG, T., 2012, "Milankovitch and sub-Milankovitch cycles of the early Triassic Daye Formation, South China and their geochronological and paleoclimatic implications" *Gondwana Res.* 22, 748–759.

WU, H., ZANG, S., HINNOV, L.A., JIANG, G., FENG, Q., LI, H., YANG, T., 2013, "Time-calibrated Milankovitch cycles for the late Permian" *Nature Communications*, 4(1), 2452.<https://doi.org/10.1038/nature06588>.